CHEMISTRY AND CATALYSIS OF COAL LIQUEFACTION: CATALYTIC AND THERMAL UPGRADING OF COAL LIQUID AND HYDROGENATION OF CO TO PRODUCE FUELS. QUARTERLY PROGRESS REPORT, JULY-SEPTEMBER 1983

UTAH UNIV., SALT LAKE CITY. DEPT. OF MINING AND FUELS ENGINEERING

OCT 1983

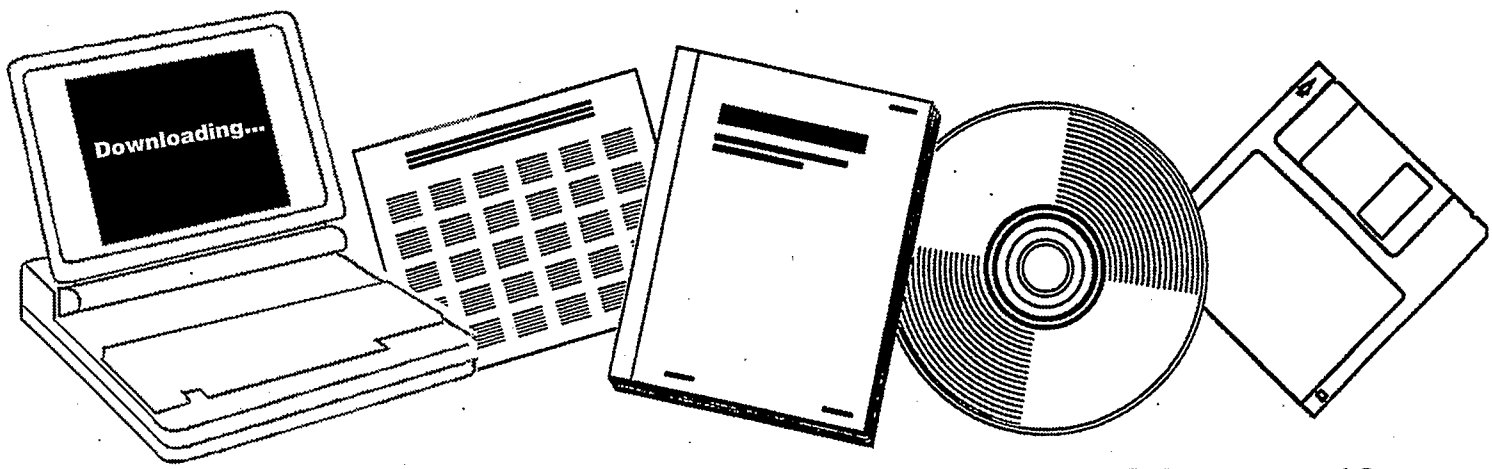

DOE/ET/14700-16
(DE84002158)
Distribution Category UC-90d

DE84002158

Chemistry and Catalysis of Coal Liquefaction Catalytic and Thermal Upgrading of Coal Liquid and Hydrogenation of CO to Produce Fuels

Quarterly Progress Report
for the Period July-Sept 1983

Dr. Wendell H. Wiser

University of Utah - Department of
Mining and Fuels Engineering
Salt Lake City, Utah 84112

Date Published - October 1983

Prepared for the United States Department
of Energy
Under Contract No. DE-AC22-79ET14700

CONTENTS

OBJECTIVE AND SCOPE OF WORK

I. The chemistry and Catalysis of Coal Liquefaction

Task 1 Chemical-Catalytic Studies

Coal will be reacted at subsoftening temperatures with selective reagents to break bridging linkages between clusters with minimal effect on residual organic clusters. The coal will be pretreated to increase surface area and then reacted at 25 to 350°C. Reagents and catalysts will be used which are selective so that the coal clusters are solubilized with as little further reaction as possible.

Task 2 Carbon-13 NMR Investigation of CDL and Coal

Carbon-13 NMR spectroscopy will be used to examine coal, coal derived liquids (CDL) and residues which have undergone subsoftening reactions in Task 1 and extraction. Improvements in NMR techniques, such as crosspolarization and magic angle spinning, will be applied. Model compounds will be included which are representative of structural units thought to be present in coal. Comparisons of spectra from native coals, CDL and residues will provide evidence for bondings which are broken by mild conditions.

Task 3 Catalysis and Mechanism of Coal Liquefaction

This fundamental study will gain an understanding of metal salt chemistry and catalysis in coal liquefaction through study of reactior known in organic chemistry. Zinc chloride and other catalytic materials will be tested as Friedel-Crafts catalysts and as redox catalysts using coals and selected model compounds. Zinc chloride, a weak Friedel-Crafts catalyst, will be used at conditions common to coal liquefaction to participate in well defined hydrogen transfer reactions. These experiments will be augmented by mechanistic studies of coal hydrogenation using high pressure thermogravimetric analysis and structural analysis. The results of these studies will be used to develop concepts of catalysis involved in coal liquefaction.

Task 4 Momentum Heat and Mass Transfer in CoCurrent Flow of Particle-Gas Systems for Coal Hydrogenation

A continuation of ongoing studies of heat and transport phenomena in cocurrent, co-gravity flow is planned for a one-year period. As time and development of existing work permits, the extension of this study to include a coiled reactor model will be undertaken. Mathematical models of coal hydrogenation systems will utilize correlations from these straight and coiled reactor configurations.

Task 5 The Fundamental Chemistry and Mechanism of Pyrolysis of Bituminous Coal

Previous work at the University of Utah indicates that coal pyrolysis, dissolution (in H-donor) and catalytic hydrogenation all have similar rates and activation energies. A few model compounds will be pyrolyze in the range of 375 to 475°C. Activation energies, entropies and pro-

duct distributions will be determined. The reactions will assist in formulating the thermal reaction routes which also can occur during hydro-liquefaction.

II. Catalytic and Thermal Upgrading of Coal Liquids

Task 6 Catalytic Hydrogenation of CD Liquids and Related Polycyclic Aromatic Hydrocarbons

A variety of coal derived (CD) liquids will be hydrogenated with sulfided catalysts prepared in Task 10 from large pore, commercially available supports. The hydrogenation of these liquids will be systematically investigated as a function of catalyst structure and operating conditions. The effect of extent of hydrogenation will be the subject of study in subsequent tasks in which crackability and hydropyrolysis of the hydrogenated product will be determined. To provide an understanding of the chemistry involved, model polycyclic arenes will be utilized in hydrogenation studies. These studies and related model studies in Task 7 will be utilized to elucidate relationships between organic reactants and the structural-topographic characteristics of hydrogenation catalysts used in this work.

Task 7 Denitrogenation and Deoxygenation of CD Liquids and Related Nitrogen- and Oxygen-Containing Compounds

Removal of nitrogen and oxygen heteroatoms from CD liquids is an important upgrading step which must be accomplished to obtain fuels corresponding to those from petroleum sources. Using CD liquids as described in Task 6, exhaustive HDN and HDO will be sought through study of catalyst systems and operating conditions. As in Task 6, catalysts will be prepared in Task 10 and specificity for N- and O-removal will be optimized for the catalyst systems investigated. Model compounds will also be systematically hydrogenated using effective HDN/HDO catalysts. Kinetics and reaction pathways will be determined. A nonreductive denitrogenation system will be investigated using materials which undergo reversible nitridation. Conditions will be sought to cause minimal hydrogen consumption and little reaction of other reducible groups.

Task 8 Catalytic Cracking of Hydrogenated CD Liquids and Related Polycyclic Naphthenes and Naphthenoaromatics

Catalytic cracking of hydrogenated CD liquid feedstocks will be studied to evaluate this scheme as a means of upgrading CD liquids. Cracking kinetics and product distribution as a function of preceding hydrogenation will be evaluated to define upgrading combinations which require the minimal level of CD liquid aromatic saturation to achieve substantial heteroatom removal and high yields of cracked liquid products. Cracking catalysts to be considered for use in this task shall include conventional zeolite-containing catalysts and large-pore molecular sieve, CLS (cross-linked smectites) types under study at the University of Utah. Model compounds will be subjected to tests to develop a mechanistic understanding of the reactions of hydro CD liquids under catalytic cracking conditions.

Task 9 Hydropyrolysis (Thermal Hydrocracking) of CD Liquids

Heavy petroleum fractions can be thermally hydrocracked over a specific range of conditions to produce light liquid products without excessive hydrogenation occurring. This noncatalytic method will be applied to a variety of CD liquids and model compounds, as mentioned in Task 6, to determine the conditions necessary and the reactibility of these CD feedstocks with and without prior hydrogenation and to derive mechanism and reaction pathway information needed to gain an understanding of the hydropyrolysis reactions. Kinetics, coking tendencies and product compositions will be studied as a function of operating conditions.

Task 10 Systematic Structural-Activity Study of Supported Sulfide Catalysts for Coal Liquids Upgrading

This task will undertake catalyst preparation, characterization and measurement of activity and selectivity. The work proposed is a fundamental study of the relationship between the surface-structural properties of supported sulfide catalysts and their catalytic activities for various reactions desired. Catalysts will be prepared from commercially available. Supports composed of alumina, silica-alumina, silica-magnesia and silica-titania, modification of these supports to change acidity and to promote interaction with active catalytic components is planned. The active constituents will be selected from those which are effective in a sulfided state, including but not restricted to Mo, W, Ni and Co. The catalysts will be presulfided before testing. Catalyst characterization will consist of physico-chemical property measurements and surface property measurements. Activity and selectivity tests will also be conducted using model compounds singly and in combination.

Task 11 Basic Study of the Effects of Coke and Poisons on the Activity of Upgrading Catalysts

This task will begin in the second year of the contract after suitable catalysts have been identified from Tasks 6, 7 and/or 10. Two commercial catalysts or one commercial catalyst and one catalyst prepared in Task 10 will be selected for a two-part study, (1) simulated laboratory poisoning/coking and (2) testing of realistically aged catalysts. Kinetics of hydrogenation, hydrodesulfurization, hydrodenitrogenation and hydrocracking will be determined before and after one or more stages of simulated coking. Selected model compounds will be used to measure detailed kinetics of the above reactions and to determine quantitatively how kinetic parameters change with the extent and type of poisoning/coking simulated. Realistically aged catalysts will be obtained from coal liquids upgrading experiment from other tasks in this program or from other laboratories conducting long-term upgrading studies. Deactivation will be assessed based on specific kinetics determined and selective poisoning studies will be made to determine characteristics of active sites remaining.

Task 12 Diffusion of Polyaromatic Compounds in Amorphous Catalyst Supports

If diffusion of a reactant species to the active sites of the catalyst is slow in comparison to the intrinsic rate of the surface reaction, then only sites near the exterior of the catalyst particles will be utilized effectively. A systematic study of the effect of molecular size on the sorptive diffusion kinetics relative to pore geometry will

be made using specific, large diameter aromatic molecules. Diffusion studies with narrow boiling range fractions of representative coal liquid will also be included. Experimental parameters for diffusion kinetic runs shall include aromatic diffusion model compounds, solvent effects, catalyst sorption properties, temperature and pressure.

III. Hydrogenation of CO to Produce Fuels

Task 13 Catalyst Research and Development

Studies with iron catalysts will concentrate on promoters, the use of supports and the effects of carbiding and nitriding. Promising promoters fall into two classes: (1) nonreducible metal oxides, such as CaO, K_2O, Al_2O_3 and MgO, and (2) partially reducible metal oxides which can be classified as co-catalysts, such as oxides of Mn, Mo, Ce, La, V, Re and rare earths. Possible catalyst supports include zeolites, alumina, silica, magnesia and high area carbons. Methods of producing active supported iron catalysts for CO hydrogenation will be investigated, such as development of shape selective catalysts which can provide control of product distribution. In view of the importance of temperature, alternative reactor systems (to fixed bed) will be investigated to attain better temperature control. Conditions will be used which give predominately lower molecular weight liquids and gaseous products.

Task 14 Characterization of Catalysts and Mechanistic Studies

Catalysts which show large differences in selectivity in Task 13 will be characterized as to surface and bulk properties. Differences in properties may provide the key to understanding why one catalyst is superior to another and identify critical properties, essential in selective catalysts. Factors relating to the surface mechanism of CO hydrogenation will also be investigated. Experiments are proposed to determine which catalysts form "surface" (reactive) carbon and the ability of these catalysts to exchange C and O of isotopically labelled CO. Reactions of CO and H_2 at temperatures below that required for CO dissociation are of particular interest.

Task 15 Completion of Previously Funded Studies and Exploratory Investigations

This task is included to provide for the orderly completion of coal liquefaction research underway in the expiring University of Utah contract, EX-76-C-01-2006.

III Highlights to Date

Task 10 Interaction effects between model reactions of binary mixtures representative of HDS, HDO, HDN and hydrogenation, using a sulfided CoMo/Al_2O_3 catalyst, were found to decrease individual reactivities in the order: N-compound > S-compound > O-compound > aromatic hydrocarbon. These result show that separate model compound reaction studies are insufficient to properly evaluate the various catalytic functionalities present on different sulfided catalysts.

Papers and Presentations

"Restrictive Diffusion in Aluminas," A. Chantong and F.E. Massoth, AICHE J. 29, 725 (1983).

Paper presented at the 1983 International Conference on Coal Science, Wednesday, August 17, 1983, Pittsburgh, Pennsylvania. "Coal Conversion at Subsoftening Conditions: Predictions of Successful Catalysts Using the HSAB Principle," by T.C. Miin and Larry Anderson.

Task 1

Comparison of Catalysts for Coal Conversion at Subsoftening Conditions

Faculty Advisor: L.L. Anderson
Graduate Student: T.C. Miin

Introduction

Catalytic coal liquefaction at subsoftening conditions by applying the HSAB principle was concluded, and a paper was presented at the 1983 International Coal Conference, which was held in Pittsburgh in August. Our work in the area of liquefaction of coal at subsoftening conditions has been reevaluated after an extensive literature search. The previously proposed mechanism cited in the penultimate report has been revised and is presented in this report.

Project Status

Ether linkage cleavage is believed to be the key step in catalytic coal liquefaction at subsoftening conditions. The detailed mechanism for the explanation of the results obtained from our experiments is as follows:

First step: Lewis Acid-Base adduct formation:

$$A + Coal \longrightarrow A^{\delta-}Coal^{\delta+}$$

Example 1. $SnCl_4 + Ar\text{-}O\text{-}R \longrightarrow Ar\text{—}O^{\delta+}\text{—}R$ (with $Sn^{\delta-}Cl_4$ coordinated to O)

The bond formation is a "sigma nonbonding-π-antibonding" interaction, as termed by the MO (molecular orbital) theory. This HOMO-LUMO (highest occupied MO - lowest unoccupied) interaction is favored thermodynamically.[1] Experimentally this was shown by Beall.[2,3]

After the formation of this acid-base adduct, the bond strength in the vicinity was altered. Gutmann's first rule[4] deals with bond-length variations and states that the smaller the intermolecular distance B → A between the donor and acceptor atoms, resulting from acid-base addition interaction, the greater the induced lengthening of the adjacent intramolecular bonds (bond weakening) in both the base and acid species. In the case of Example 1, the bonding strength is varied as:

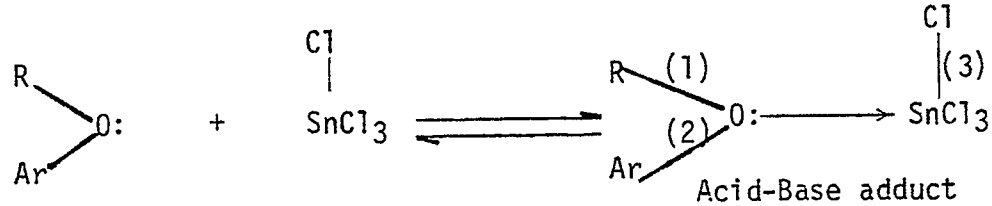

Acid-Base adduct

Note that bonds (1), (2), and (3) are lengthened (weakened). The weakened ether linkage, for example, is more easily susceptible to hydrogenolysis.

Although the formation of the above acid-base adduct has indeed occurred, another acid-base adduct can also be formed. This reaction is the associated proton-Lewis base adduct formation:

Example 2. $SnCl_4 + H_2O \rightleftharpoons H^{\delta+}(OHSnCl_4)^{\delta-}$

$$H^{\delta+}(OHSnCl_4)^{\delta-} + Ar - O - R \rightleftharpoons Ar - O - R$$
$$\downarrow$$
$$(OHSnCl_4)^{\delta-}H^{\delta+}$$

Both above reactions are acid-base adduct formation. The first reaction is the so-called Bronsted form of the Lewis Acid. Since there is no massive quantity of water in coal liquefaction reactions, the Bronsted Acid formed should be closely associated with its precursor Lewis Acid. Since weak acids can not accept donor species to a great extent, water molecules are believed to be dissociated only to a small extent. This can be understood more clearly by Gutmann's first rule:

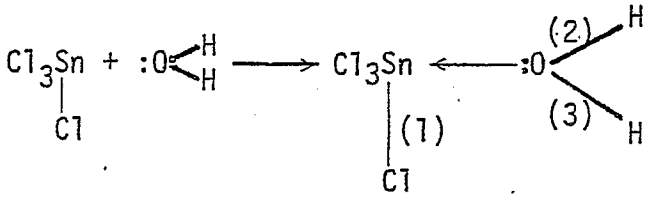

Again, due to the formation of acid-base adduct, vicinal bonds (1), (2) and (3) are weakened. The two hydrogen atoms in water are still held by oxygen-hydrogen bonds rather than dissociated fully to form protons. However, when another bond, i.e., an ether linkage in the coal structure, enters the reaction, the bonding strength of the O—H bonds are weakened further:

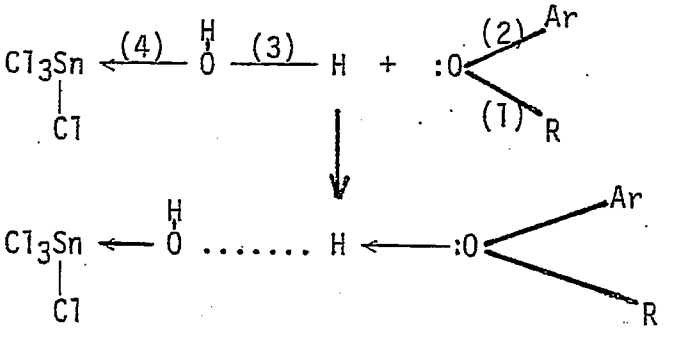

It is interesting to note that bonds (1), (2) and (3) are weakened as explained before. However, bond (4) is strengthed according to Gutmann's 2nd rule.[5] The total effect on the O—H bond is that it is weakened twice, that is, it is almost certainly is cleaved. (But it is still associated by its counter ion due to hydrogen bonding.)

The above two adducts have been compared to determine which provided the weakest ether linkages in the coal structure. The redrawing of these two adducts can be shown thus:

Lewis Acid-coal adduct:

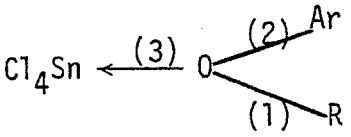

Lewis Acid in Bronsted form-coal adduct:

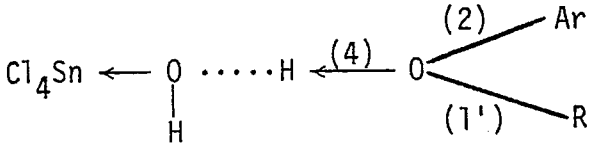

The weaker ether linkages, Bonds (1) and (2), depend on stronger adduct bonds (according to Gutmann's first rule). According to the HSAB Principle Bond (4) is stronger than Bond (3), because the hardness between H and O is more similar than the hardness between Sn and O. Therefore, Bond (1') is weaker than Bond (1). The conclusion is that the Bronsted form of the Lewis Acid is favored for coal liquefaction at subsoftening conditions.

An explanation of why the Borderline Lewis Acids are better catalysts follows. Three examples of a Lewis Acid-coal adduct (in their Bronsted form) are:

Hard Lewis Acid-coal adduct:

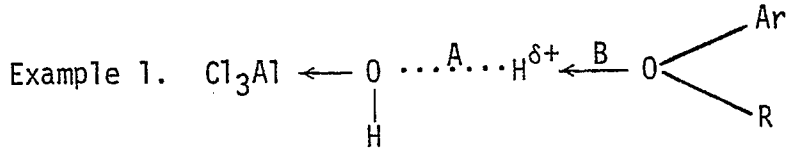

Borderline Lewis Acid-coal adduct:

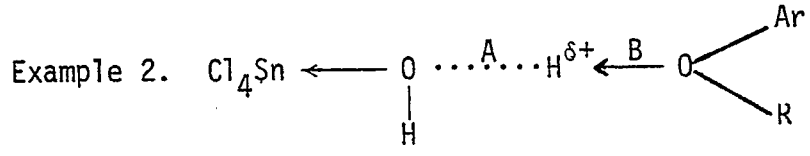

Soft Lewis Acid-coal adduct:

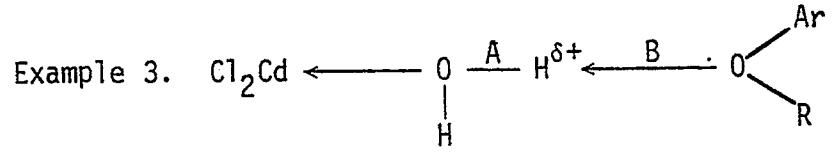

When applying the HSAB Principle to the three examples above, the oxygen-metal bond in Example 1 is the strongest, whereas the O-H (A) bond in Example 1 is the weakest. The partial positive charge on the hydrogen atom is the greatest, which in turn forms the strongest oxygen-hydrogen bond (B) between ether linkage and hydrogen. This means that Example 1 represents the weakest ether bonding structure in the three coal-catalyst adducts mentioned above. However, the weakened ether functional groups can have other side reactions (e.g., Scholl condensation, Friedal-Craft alkylation, etc.)[6] competing with the hydrogenolysis reaction. The labile surroundings of the ether linkage and the favorable entropy factors favor the occurence of side reactions. Massive char production during hard acid catalyzed coal liquefaction is evidence of this proposed mechanism. Hard acids cause weakened ether linkages, but the weakened ether linkage is too active for hydrogenolysis to occur. However, soft acids cause the ether linkages to weaken to a lesser extent and, thus, the soft acids are inadequate in activity to favor further reactions. Only borderline acids provide appropriate weakening and thus promote hydrogenolysis.

Future Work

Lewis Base catalyzed coal liquefaction studies will be done. The effect of different mixtures of Lewis Acids and Lewis Bases catalyzed coal liquefaction reactions will also be studied.

Reference

1. W. Jensen, "The Lewis Acid-Base Concept," Wiley, New York, New York, 1980, Chapter 3.

2. H. Beall, Fuel, 58, 319 (1979).

3. ibid, 62, 289 (1983).

4. W. Jensen, "The Lewis Acid-Base Concepts," Wiley, New York, New York, 1980, p 135.

5. ibid., p 136

6. A.T. Bell, Fuel, 61, 745 (1982).

Task 2

Carbon-13 NMR Investigation of CDL and Coal

Faculty Advisor: R.J. Pugmire
Postdoctor: A. Beeler

Introduction

Work has continued to be delayed by the loss of personnel. Dr. Woolfenden has taken a job in industry. A new Ph.D., Alvin Beeler, joined the project on September 1, 1983 and is in the process of orienting himself to the project.

Project Status

The data on the Exxon sample set have not been completely analyzed. This will be one of the first assignments of Dr. Beeler.

Previously unreported results were recently published.[1] This work was carried out in collaboration with Dr. Michael A. Wilson of CSIRO.

Reference

1. M.A. Wilson, R.J. Pugmire, A.M. Vassallo, D.M. Grant, P.J. Collin and K.W. Zilm, I&EC Product Research & Development, 21, 477 (1982).

Task 3

Catalysis and Mechanism of Coal Liquefaction

Faculty Advisor: D.M. Bodily
Graduate Student: Tsejing Ray

Introduction

Metal halides such as $ZnCl_2$ are well-known to be active catalysts for coal hydrogenation. Zinc chloride has been shown to be a very effective catalyst for coal hydrogenation in the entrained-flow reactor developed at the University of Utah.[1,2] Bell and co-workers[3-5] have studied the reactions of model compounds with $ZnCl_2$ under conditions similar to those employed in coal hydrogenation. They observed cleavage of C-O and C-C bonds in the model compound and proposed that the active catalytic species is a Bronsted acid formed $ZnCl_2$.

Shibaoka, Russell and Bodily[6] proposed a model to explain the liquefaction of coal, based on microscopic examination of the solid products from metal halide catalyzed coal hydrogenation. The model involves a competition between hydrogenation and carbonization reactions. The hydrogenation process starts at the surface of vitrinite particles and progresses toward the center. The vitrinite is converted to a plastic material of lower reflectance, which is the source of oils, asphaltenes and preasphaltenes. Concurrently, carbonization occurs in the center of the particles, resulting in vesiculation and a higher reflectance material. The partially carbonized material can be hydrogenated at later stages, but at a lower rate than the original coal.

Thermal and/or catalytic bond rupture occurs during the liquefaction process. The initial products of the bond cleavage reactions may be stabilized by hydrogen addition, resulting in cleavage of bridges between aromatic ring systems and in dealkylation of aromatic rings. If the initial products of the reaction are not stabilized, they may polymerize to form semicoke-like material. This primary semicoke may be isotropic or exhibit a fine-grained anisotropic mosiac texture, depending on the rank of coal. The plastic material formed by stabilization of the initial products may be further hydrogenated or, under hydrogen deficient conditions, may form secondary semicoke. The secondary semicoke is of medium to coarse-grained anisotropic mosiac texture. Bodily and Shibaoka[7] used this model to explain the nature of the residues from hydrogenation in the short-residence, entrained-flow hydrogenation reactor. The role of the $ZnCl_2$ catalyst is examined in this study.

The Clear Creek (high volatile bituminous) coal and Coal Basin (medium volatile bituminous) coal samples heated in hydrogen and in nitrogen were analyzed by optical microscopy. Results of the analysis were previously reported. In hydrogen the $ZnCl_2$ catalyst causes an obvious softening of the coal grains at 350°C. At short reaction times, a reacted rim is observed on the grains. At 20 minutes reaction time and 400°C, the reacted zone is not visible, indicating that the reaction has proceeded through the entire grain. The initial reactions involve softening of the

vitrinite and reaction of exinites. When $ZnCl_2$ is not present, only slight softening occurs prior to carbonization.

In nitrogen, the $ZnCl_2$ also appears to increase the fluidity of the sample during heating, although not to the same extent as in hydrogen. This effect shows up in the size and shape of vesicules.

Project Status

Under fluorescent microscopic examination, the exinite component of Clear Creek coal showed a yellow color under fluorescent light conditions. At temperatures below 400°C, the exinite persisted in the coal grains in most cases as shown in Tables 1-4. At higher temperatures the exinite is almost gone beyond 450°C, especially for the coal-impregnated with $ZnCl_2$ catalyst.

Oya et al.[8] presented a classification system to describe the optical texture of anisotropic coke. Residues of heat-treated Coal Basin coal showed anisotropic character under polarizing light. This system was used to describe coal residues of these cokes. Anisotropic regions are described as fine-grained mosaics (size less than 1.5 μm), medium-grained mosaics (size 1.5-5.0 μm), coarse-grained mosaics (size 5.0-∿10.0 μm), small domains and domains. Uncatalyzed samples have a larger percentage of mosaics than catalyzed samples (Figures 1-4). After heating in the higher temperature region (500°C), the catalyzed system tends to have higher compositions of domain structures.

The reflectance of Clear Creek coal heat-treatment residues was measured. Catalyzed samples after hydrotreatment (from 350-500°C) showed gradually increasing reflectance. The catalyzed system showed similar trends but with higher reflectance and sharper differences in each step. After nitrogen treatment at 350-500°C, the reflectance increased, but drops down after heating at 500°C in both cases of the catalyzed and uncatalyzed samples (Figures 5 and 6).

Future Work

The observations and experimental data will be further analyzed and interpreted and a final report prepared.

References

1. R.E. Wood and W.H. Wiser, Ind. Eng. Chem., Proc. Design Devel., 15, 144 (1976).
2. J.M. Lytle, R.E. Wood and W.H. Wiser, Fuel, 59, 471 (1980).
3. D.P. Mobley and A.T. Bell, Fuel, 58, 661 (1979).
4. N.D. Taylor and A.T. Bell, Fuel, 59, 499 (1980).
5. D.P. Mobley and A.T. Bell, Fuel, 59, 507 (1980).
6. M. Shibaoka, N.J. Russell and D.M. Bodily, Fuel, 61, 201 (1982).

7. D.M. Bodily and M. Shibaoka, Fuel, submitted.

8. A. Oya, Z. Qian and H. Marsh, Fuel, 62, 274 (1983).

Table 1. Fluorescent microscopy of Clear Creek, Utah coal heated in hydrogen.

Temp., °C	Without Catalyst	With Catalyst
400	Yellow strip observed	Many yellow strips
450	Yellow spots exist	Only traces of yellow spots
500	Almost no yellow color	Almost no yellow spots

Table 2. Fluorescent microscopy of Clear Creek, Utah coal heated in nitrogen.

Temp., °C	Without Catalyst	With Catalyst
400	Many yellow strips observed	Trace yellow spots
450	No yellow spots found	No yellow spots found
500	Almost no yellow spots found	No yellow spots found

Table 3. Fluorescent microscopy of Coal Basin, Colorado coal heated in hydrogen.

Temp., °C	Without Catalyst	With Catalyst
400	Some yellow blocks	Some yellow spots
450	Yellow spots observed	Few yellow spots found
500	Only tiny brownish-yellow spots exist	Some yellow spots exist

Table 4. Fluorescent microscopy of Coal Basin, Colorado coal heated in nitrogen.

Temp., °C	Without Catalyst	With Catalyst
400	Trace of yellow spots	No yellow spots
450	Yellow spots exist	Trace yellow spots
500	Some yellow spots found	No yellow spots

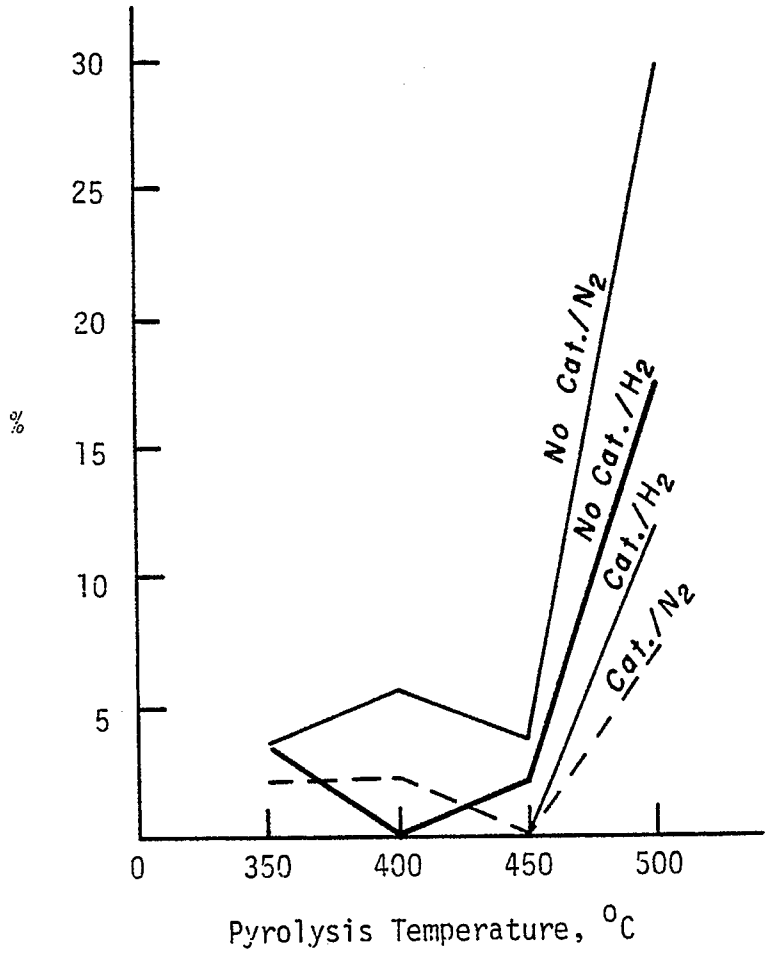

Figure 1. The fine-grained mosaic distribution of Coal Basin, Colorado Coal.

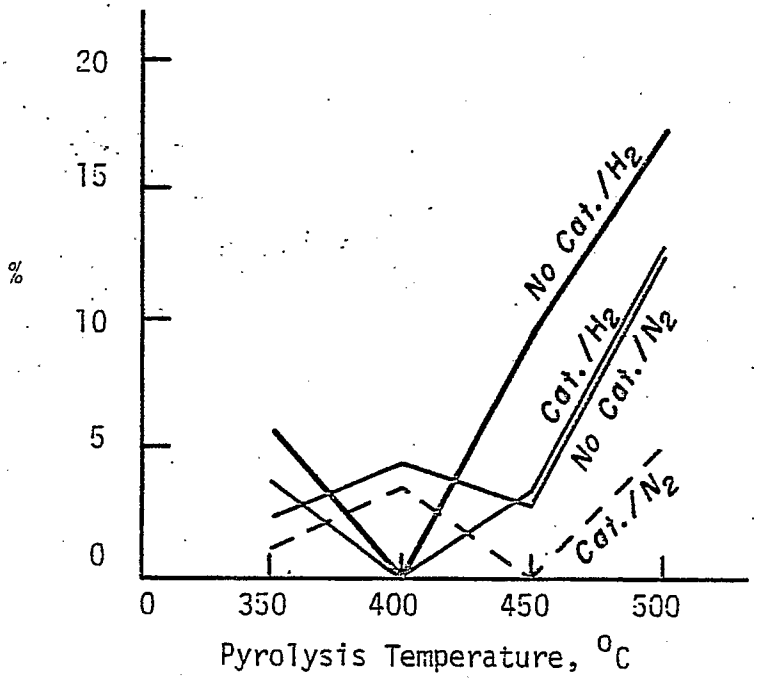

Figure 2. The medium-grained mosaic distribution of Coal Basin, Colorado Coal.

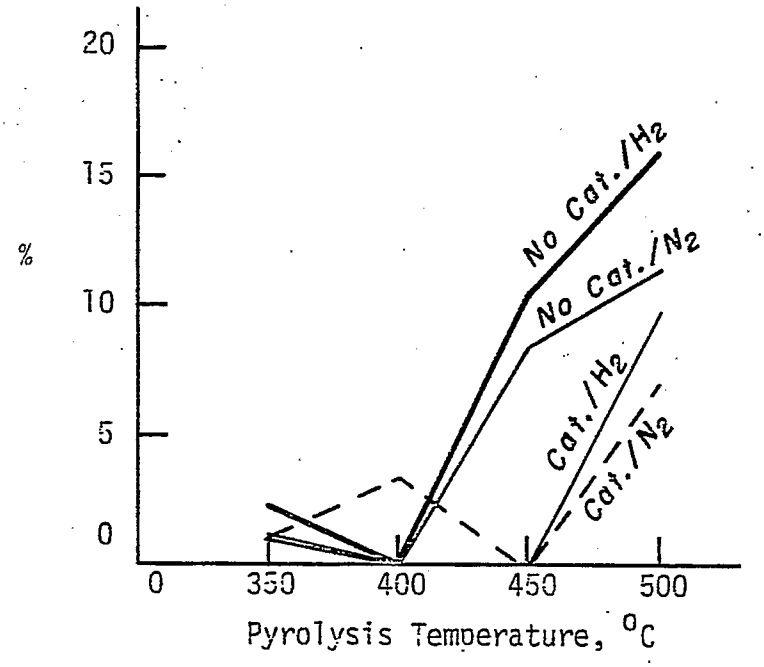

Figure 3. The coarse-grain mosaic distirbution of Coal Basin, Colorado Coal.

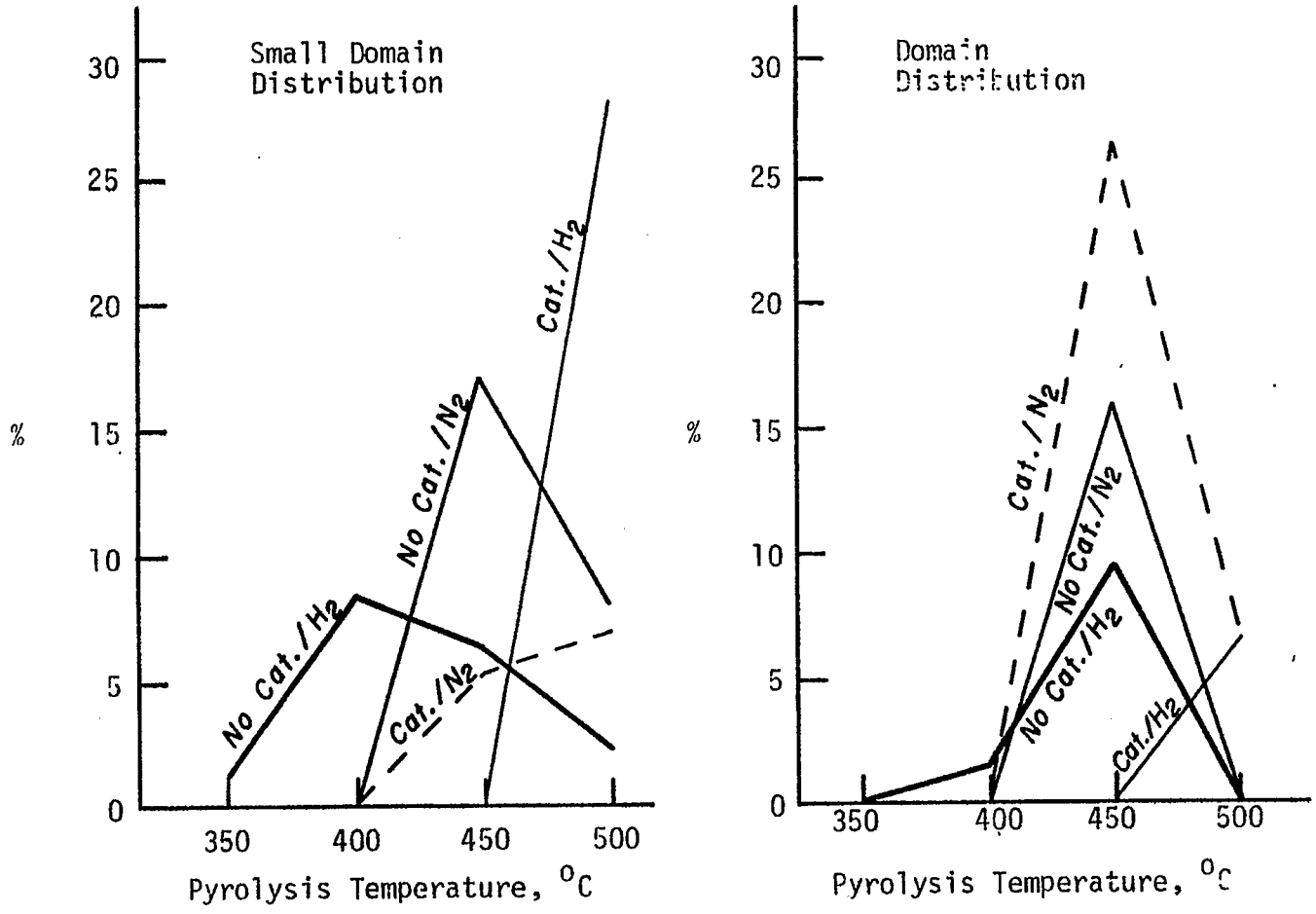

Figure 4. The domain distribution of Coal Basin, Colorado Coal.

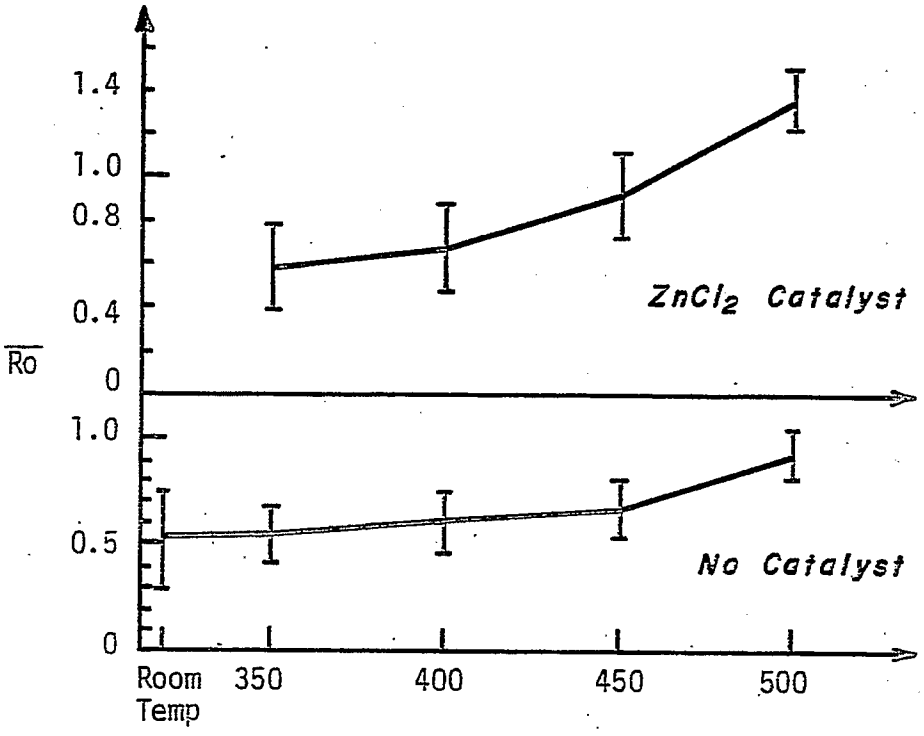

Figure 5. The reflectance of Clear Creek, Utah coal after hydrogenolysis.

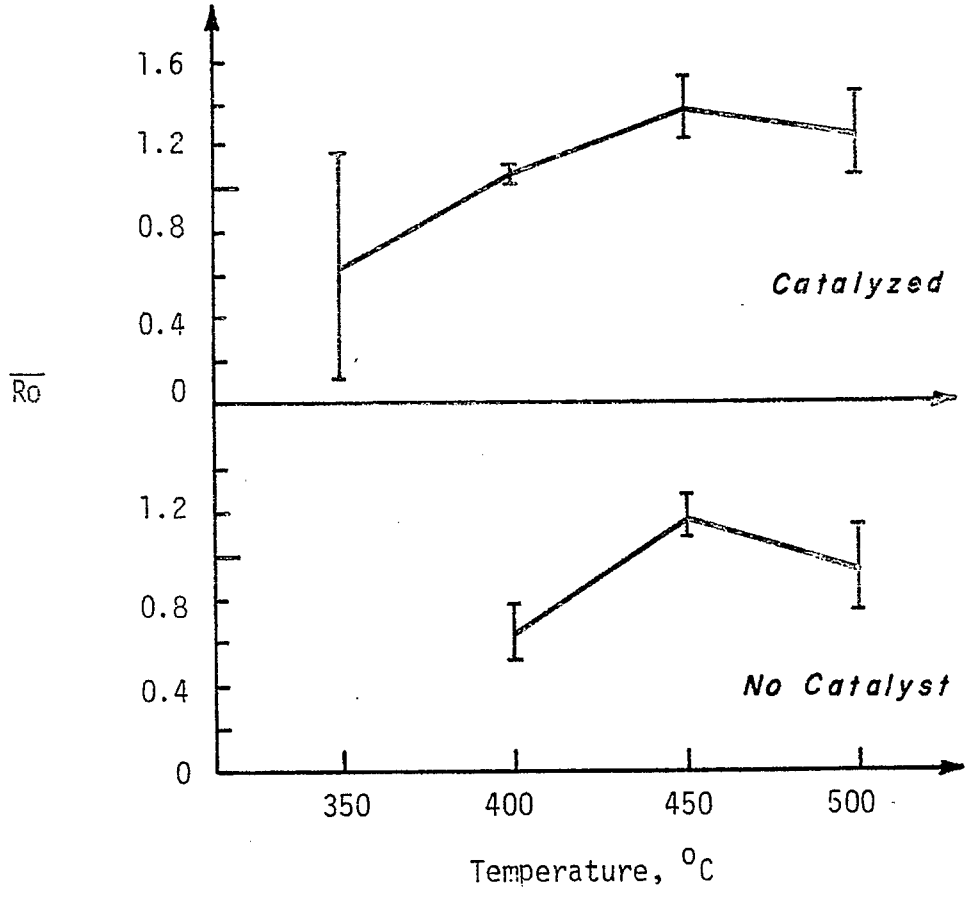

Figure 6. The reflectance of Clear Creek, Utah coal after pyrolysis.

Task 5

The Mechanism of Pyrolysis of Bituminous Coal

Faculty Advisor: W.H. Wiser
Graduate Student: J.K. Shigley

Introduction

In the present state of knowledge concerning the fundamental chemistry of coal liquefaction in the temperature range 375-550°C, the liquefaction reactions are initiated by the thermal rupture of bonds in the bridges joining configurations in the coal, yielding free radicals. The different approaches to liquefaction, except for Fischer-Tropsch variations, represent ways of stabilizing the free radicals to produce liquid-size molecules. The stabilization involving abstraction by the free radicals of hydrogen from the hydroaromatic structures of the coal is believed to be the predominant means of yielding liquid size molecules in the early stages of all coal liquefaction processes, except Fischer-Tropsch variations. The objective of this research is to understand the chemistry of this pyrolytic operation using model compounds which contain structures believed to be prominant in bituminous coals.

Project Status

The pyrolysis of 1-benzyl-1,2,3,4-tetrahydroisoquinoline (1-BTHIQ) has been conducted at 638 and 588 Kelvin (365 and 315°C). The conversion and material balance results are shown in Tables 1 and 2. The normalized product distribution data are tabulated in Tables 3 and 4 and plotted in Figures 1 and 2. The trends exhibited by 1-BTHIQ, as discussed in the previous report, are very similar to those of 9-benzyl-1,2,3,4-tetrahydrocarbazole (9-BTHC).[1]

The results of the kinetic analysis using the integral technique are shown in Tables 5 and 6. The first order kinetic plots are shown in Figures 3 and 4, and the second order kinetic plots are shown in Figures 5 and 6. The data at 638 K (365°C) are best modeled by first order overall kinetics. The lower temperature data, 588 K (315°C), seem to be described best by second order overall kinetics.

The development of an analysis procedure for 1-piperidinomethyl-2-naphthol (1-PMN) has been attempted.[1] Problems were encountered with the apparent decomposition of 1-PMN upon injection. Numerous gas chromatographic columns were utilized in an attempt to facilitate its use as a model compound. A survey of pertinent literature and discussions with gas chromatography experts were fruitless. No column was found which would allow 1-PMN to be used in this pyrolysis study.

The 4-benzylpiperidine (4-BPP) has been pyrolyzed at 673 K (400°C).[1] Its behavior upon pyrolysis is significantly different than that of 1-BTHIQ and 9-BTHC. The product analysis by gas chromatography has proven to be very complicated and frustrating. The major difficulty has been with the

separation of toluene and piperidine. Several GC columns (6) were tried before finding an appropriate column. No pertinent information was found in the literature. The column found which works for this separation is: 5% carbowax 20M + 0.8% KOH on 60/80 Carbopack B, in a 6 ft long by 1/4 inch (2 mm I.D.) glass column. A complication with this column is the long retention time of 4-BPP and 4-benzylpyridine (approximately 45 and 57 minutes).

The results of the pyrolysis of 4-BPP are shown in Tables 7, 8 and 9. The normalized product distribuion is shown in Figure 7. The first and second order overall kinetics plots are shown in Figures 8 and 9. A definite conclusion regarding the overall kinetics and mechanism of 4-BPP pyrolysis is not appropriate at this time.

Preliminary results from the pyrolysis of 4-BPP at 723 K (450°C) suggests that the piperdine ring is subject to deterioration at this temperature, especially at higher conversions of 4-BPP.

Vapor-liquid equilibrium estimations have been made for 9-BTHC and 1-BTHIQ at their pyrolysis temperatures. Utilizing vapor pressure data from the literature, a correlation of Ln P vs. 1/T was developed. Vapor pressures for the compounds were estimated at the pyrolysis temperatures and utilized to estimate the vapor-liquid equilibrium of the model compounds at the temperatures of pyrolysis. The results of this analysis are shown in Tables 10 and 11. It must be recognized that these are estimations, and errors of 5-10% are not improbable. Also, where it is shown that one-hundred percent of the compound is in either the vapor or liquid phase, it should be understood that a small amount of the compound (< 1%) will also be present in the liquid or vapor phase, respectively. Since the estimations are not thought to be within 1%, they are listed as fractions of the total model compound present. It is interesting to note that the overall reaction order undergoes a transition from two to one as the model compound goes from approximately the liquid or vapor phase.

Estimates of the chemical equilibrium of 9-BTHC and its observed pyrolysis products, 9-benzylcarbazole (9-BC), carbazole (CARB), 1,2,3,4-tetrahydrocarbazole (THC) and toluene (TOL) have been made. The methods of Benson[2,3,4] were utilized to estimate values for $\Delta H^{o}_{F,T}$, ΔS^{o}_{T} and $C^{o}_{p\,T}$. These values were then used to calculate $\Delta G_{F,T}$ and $\Delta G_{RXN,T}$. The reaction utilized was:

$$3(9\text{-BTHC}) \rightleftharpoons 9\text{-BC} + \text{THC} + \text{CARB} + 2(\text{TOL}) + 2H_2$$

If a basis of 3 moles of 9-BTHC is assumed, with none of the products present initially and Z is assumed to be the extent of reaction of 9-BTHC, an expression for the equilibrium constant can be derived. The resultant expression is:

$$K_{EQ} = \frac{0.1975\ Z^7}{(3-Z)^3(1-2Z)^4}$$

The results of this analysis, the estimated $\Delta G^{o}_{RXN,T}$, K_{EQ} and Z are shown in Table 12. As can be seen, at temperatures above 648 K (375°C), almost complete conversion of 9-BTHC is favored thermodynamically. However, the time-frame for this process to occur is controlled by the kinetic pathway. This analysis has shown that in the pyrolysis of 9-BTHC the kinetics are the controlling factor.

Future Work

Gas chromatographic/mass spectrometric analyses of the pyrolysis products of 1-BTHIQ and 4-BPP will be conducted. Further experiments will be conducted with 1-BTHIQ and 4-BPP to determine the extent of hydrogen (H_2) production. Also, pyrolysis experiments for 4-BPP will be conducted at four more temperatures.

Mathematical modeling of the pyrolysis of 9-BTHC, 1-BTHIQ and 4-BPP will be conducted utilizing the technique of time-concentration integrals.

References

1. W.H. Wiser et al., DOE Contract No. DE-AC22-79ET14700, Quarterly Progress Report, Salt Lake City, Utah, April-June 1983.

2. S.W. Benson and J.H. Buss, J. Chem. Phys. 29 (3), 546 (1958).

3. S.W. Benson et al., Chem. Rev., 68, 279 (1968).

4. S.W. Benson, "Thermochemical Kinetics," John Wiley & Sons, Inc., New York, 1968, p 18.

Table 1. Pyrolysis of 1-Benzyl-1,2,3,4-Tetrahydroisoquinoline (1-BTHIQ). Temperature: 638 Kelvin (365°C).

Reaction Time, Min	Initial Conc'n of 1-BTHIQ mmole/cc	% Material Balance	Conversion of 1-BTHIQ ± SD
1.0	0.03105	99.90	0.2615 ± 0.02
3.0	0.03179	102.7	0.6063 ± 0.008
5.0	0.03212	99.52	0.7328 ± 0.06
8.0	0.03065	102.0	0.9261 ± 0.003
10.0	0.03091	96.56	0.9545 ± 0.007
12.0	0.03136	103.8	0.9723 ± 0.001

Notes:

1. % Mat'l Balance = $\left[\frac{N(THIQ) + N(ISOQ) + N(1\text{-}BIQ) + N_A}{N_{Ao}}\right] \times 100$

2. Conversion = $\left[1 - \frac{N_A}{N_{Ao}}\right]$

3. SD = Standard deviation

where, N_A = millimoles of 1-BTHIQ @ t

N_{Ao} = millimoles of 1-BTHIQ @ t = 0

Table 2. Pyrolysis of 1-Benzyl-1,2,3,4-Tetrahydroisoquinoline (1-BTHIQ). Temperature: 588 Kelvin (315°C)

Reaction Time, Min	Initial Conc'n of 1-BTHIQ mmole/cc	% Material Balance	Conversion of 1-BTHIQ ± SD
5.0	0.03223	104.9	0.056 ± 0.0004
8.0	0.03111	101.2	0.1250 ± 0.002
10.0	0.03054	95.60	0.2231 ± 0.003
20.0	0.02920	91.02	0.3409 ± 0.027
30.0	0.03117	91.70	0.4019 ± 0.019
60.0	0.03116	94.33	0.5150 ± 0.015

Notes:

1. % Material Balance = $[\{N(THIQ) + N(ISOQ) + N(BIQ) + N_A\}/N_{Ao}] \times 100$
2. Conversion = $1-(N_A/N_{Ao})$
3. SD = Standard deviation

where, N_A = millimoles of 1-BTHIO @ t

N_{Ao}= millimoles of 1-BTHIQ @ t=0

Table 3. Pyrolysis of 1-Benzyl-1,2,3,4-Tetrahydroisoquinoline (1-BTHIQ).
Temperature: 638 Kelvin (365°C)

Reaction Time, min	Conversion of 1-BTHIQ ± SD	% Mat'l Balance	Relative Amounts (%, Normalized)					1-BIQ/ISOQ Molar Ratio
			1-BTHIQ	1-BIQ	THISOQ	ISOQ	Toluene	
1.0	0.2615 ± 0.02	99.90	53.95	20.91	9.45	3.12	12.57	6.94
3.0	0.6063 ± 0.008	102.7	22.63	19.59	23.2	5.69	28.89	3.48
5.0	0.7328 ± 0.06	99.52	15.22	17.14	27.10	6.73	33.82	2.67
8.0	0.9261 ± 0.003	102.0	4.04	16.67	28.98	10.67	39.65	1.60
10.0	0.9545 ± 0.007	96.56	2.48	12.81	30.19	12.17	42.36	1.09
12.0	0.9723 ± 0.001	103.8	1.37	11.87	30.54	12.83	43.38	0.94

Where, 1-BIQ = 1-Benzylisoquinoline

THISOQ= 1,2,3,4-Tetrahydroisoquinoline

ISOQ = Isoquinoline

Table 4. Pyrolysis of 1-Benzyl-1,2,3,4-Tetrahydroisoquinoline (1-BTHIQ).
Temperature: 588 Kelvin (315°C)

Reaction Time, min	Conversion of 1-BTHIQ ± SD	% Mat'l Balance	Relative Amounts (%, Normalized)					1-BIQ/ISOQ Molar Ratio
			1-BTHIQ	1-BIQ	THISOQ	ISOQ	Toluene	
5.0	0.0560 ± 0.0004	104.9	69.28	16.06	4.24	3.09	7.33	5.24
8.0	0.1250 ± 0.002	101.2	65.31	16.67	5.03	3.98	9.01	4.31
10.0	0.2231 ± 0.003	95.60	61.30	17.64	5.63	4.91	10.54	3.57
20.0	0.3409 ± 0.027	91.02	54.24	16.10	6.83	8.02	14.85	2.02
30.0	0.4019 ± 0.019	91.70	47.82	10.80	9.39	11.31	20.69	0.96
60.0	0.5150 ± 0.015	94.33	34.39	9.90	14.07	13.78	27.85	0.72

where, 1-BIQ = 1-Benzylisoquinoline

THISOQ = 1,2,3,4-Tetrahydroisoquinoline

ISOQ = Isoquinoline

Table 5. Pyrolysis of 1-Benzyl-1,2,3,4-Tetrahydrosioquinoline (1-BTHIQ).

Overall Reaction(s) Order Determination - Integral Technique

Temperature: 638 Kelvin (365°C)

Reaction Time, min	Kinetic Plot Ordinates: First Order $-Ln(1-x_A)$	Kinetic Plot Ordinates: Second Order $x_A/[C_{Ao}(1-x_A)]$
1.0	0.303	11.5
3.0	0.932	48.4
5.0	1.33	88.5
8.0	2.60	408.8
10.0	3.10	687.5
12.0	3.59	1121

Plot	Y-Intercept	Slope	r^2
First Order $-Ln(1-x_A)=k_1t$	-0.024	0.308	0.9917
Second Order $\frac{x_A}{C_{Ao}(1-x_A)} = k_2t$	-246.3	98.06	0.8923

where, k_1[=] min^{-1}; k_2[=] $\frac{cc}{mmole\text{-}min}$

x_A = conversion of 1-BTHIQ

C_{Ao} = initial concentration of 1-BTHIQ, mmole/cc

Table 6. Pyrolysis of 1-Benzyl-1,2,3,4-Tetrahydrosioquinoline (1-BTHIQ).

Overall Reaction(s) Order Determination - Integral Technique

Temperature: 588 Kelvin (315°C)

Reaction Time, min	Kinetic Plot Ordinates: First Order $-Ln(1-x_A)$	Kinetic Plot Ordinates: Second Order $x_A/[C_{Ao}(1-x_A)]$
5.0	0.0577	1.842
8.0	0.1336	4.595
10.0	0.2525	9.408
20.0	0.4172	17.76
30.0	0.5143	21.57
60.0	0.7238	34.10

Linear Progression Analysis

Plot	Y-Intercept	Slope	r^2
First Order $-Ln(1-x_A)=k_1t$	0.0956	0.0115	0.8997
Second Order $\frac{x_A}{C_{Ao}(1-x_A)}=k_2t$	2.36	0.5649	0.9383

Table 7. Pyrolysis of 4-Benzylpiperidine (4-BPP).
Temperature: 673 Kelvin (400°C)

Reaction Time, Min	Initial Conc'n of 4-BPP, mmole/cc	% Material Balance	Conversion of 4-BPP ± SD
10.0	0.03166	101.0	0.0392
20.0	0.03129	94.90	0.1485
	0.03045	94.65	0.1668
30.0	0.03130	90.63	0.2799
60.0	0.03101	95.72	0.2831
	0.03146	94.74	0.3078
120.0	0.03324	95.02	0.4878

Notes:

1. % Material Balance = $|(N_A + N_B + N_C + N_D + N_F + N_E)/N_{Ao}| \times 100$
2. Conversion of 4-BPP = $1-N_A/N_{Ao}$
3. SD = Standard deviation

where, N_i = millimoles of i @ t

N_{io} = millimoles i @ t=0

A = 4-BPP

B = 4-Benzylpyridine (4-BPY)

C = Piperidine (PIP)

D = Pyridine (PYD)

F = 4-Methylpiperidine (4-MPP)

G = 4-Methylpyridine (4-MPY)

Table 8. Pyrolysis of 4-Benzylpiperidine (4-BPP).
Temperature: 673 Kelvin (400°C)

Reaction Time, min	Conversion of 4-BPP ± SD	% Mat'l Balance	Relative Amounts (%, Normalized)							4-BPY/PYD Molar Ratio
			4-BPP	4-BPY	PIP	PYD	TOL	4-MPP	4-MPY	
10.0	0.0392	101.0	94.97	0.530	0.1652	4.131	4.30	0	0	0.128
20.0	0.1577 ± 0.01	94.78	79.09	0.680	0.2075	6.243	12.81	0.575	0.388	0.1096
30.0	0.2799	90.63	66.43	0.290	0.495	9.724	21.57	1.023	0.463	0.0298
60.0	0.2955 ± 0.02	95.23	60.56	0.505	0.437	10.68	26.24	1.090	0.477	0.0465
120.0	0.4878	95.02	41.56	0.550	0.397	15.89	39.02	1.856	0.737	0.0346

where, 4-BPY = 4-Benzylpyridine

PIP = Piperdine

PYD = Pyridine

TOL = Toluene

4-MPP = 4-Methylpiperidine

4-MPY = 4-Methylpyridine

Table 9. Pyrolysis of 4-Benzylpiperidine (4-BPP).

Overall Reaction(s) Order Determination - Integral Technique

Temperature: 673 Kelvin (400°C)

Reaction Time, min	Kinetic Plot Ordinates: First Order $-Ln(1-x_A)$	Kinetic Plot Ordinates: Second Order $x_A/[C_{Ao}(1-x_A)]$
10	0.0400	1.288
20	0.1607	5.573
	0.1825	6.576
30[a]	0.3284	12.417
60	0.3329	12.738
	0.3679	14.134
120	0.6690	28.651

Plot	Y-Intercept	Slope	r^2
First Order $-Ln(1-x_A)=k_1t$	0.0366	0.0053	0.9792
Second Order $\frac{x_A}{C_{Ao}(1-x_A)}=k_2t$	0.251	0.2326	0.9843

where, k_1[=] min^{-1}; k_2[=] $\frac{cc}{mmole\text{-}min}$

x_A = Conversion of 4-BPP

C_{Ao} = Initial concentration of 4-BPP, mmole/cc

[a]Excluded from Linear Regression Analysis.

Table 10. Vapor-Liquid Equilibrium Estimation for 9-BTHC.

Temp, K	Vapor Press, atm	Fraction		Observed Overall Reaction Order
		Vapor	Liquid	
633	0.582	0	1	3+
648	0.810	0	1	2
673	1.36	0.43	0.57	1.5
683	1.66	0.68	0.32	1.5
698	2.21	1	0	1.0
713	2.90	1	0	1.0

Table 11. Vapor-Liquid Equilibrium Estimation for 1-BTHIQ.

Temp, K	Vapor Press, atm	Fraction		Observed Overall Reaction Order
		Vapor	Liquid	
585	0.848	0.06	0.94	2
598	1.25	0.32	0.68	2
611	1.80	0.63	0.37	1.5
623	2.49	0.99	0.01	1.0
638	3.68	1	0	1.0

Table 12. Chemical Equilibrium Estimation for the Pyrolysis of 9-Benzyl-1;2,3,4-Tetrahydrocarbazole (9-BTHC).

Cumulative Reaction:

$$3(9\text{-BTHC}) \rightleftharpoons 9\text{-BC} + \text{THC} + \text{CARB} + 2(\text{TOL}) + 2(H_2)$$

$$\Delta G^{o}_{RXN,T} = \Delta G^{o}_{T}(9\text{-BC}) + \Delta G^{o}_{T}(\text{THC}) + \Delta G^{o}_{T}(\text{CARB}) + 2\Delta G^{o}_{T}(\text{TOL}) + 2\Delta G^{o}_{T}(H_2) - 3\Delta G^{o}_{T}(9\text{-BTHC})$$

$$= -RT \text{ Ln } K_{EQ}$$

Temp, K (^{o}C)	$\Delta G^{o}_{RXN,T}$, kcal/mole	K_{EQ}	Estimated Extent of Reaction of 9-BTHC (%)
300 (27)	15.0	0.975	75.5
633 (360)	-15.8	1.01	75.7
648 (375)	-17.3	6.89×10^{5}	99.67
673 (400)	-19.8	2.67×10^{6}	99.79
683 (410)	-20.9	4.86×10^{6}	99.83
698 (425)	-22.3	9.73×10^{6}	99.86
713 (440)	-23.9	2.05×10^{7}	99.89
1000 (727)	-54.4	7.61×10^{11}	99.997

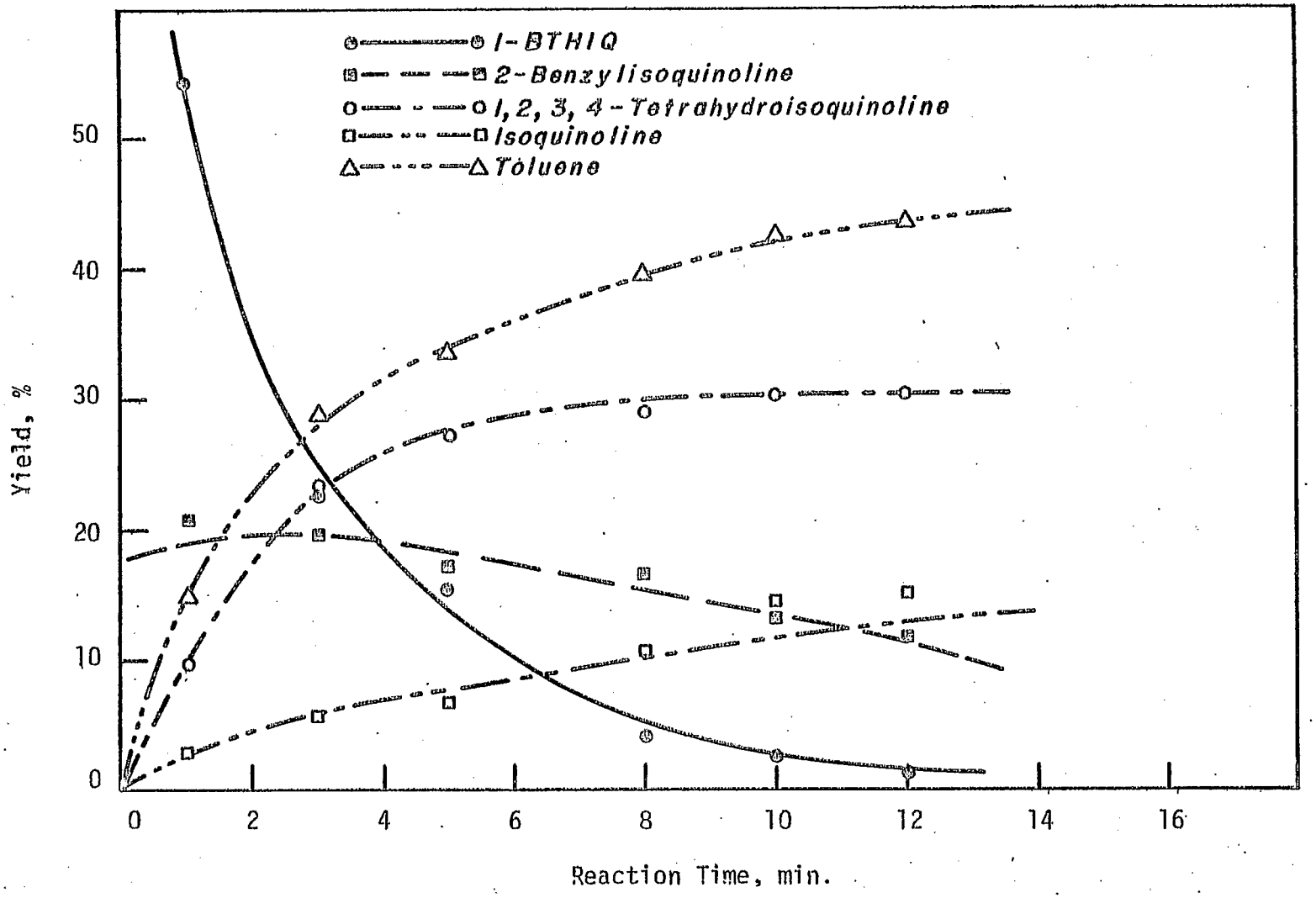

Figure 1. Pyrolysis of 1-Benzyl-1,2,3,4-tetrahydroisoquinoline (1-BTHIQ). Normalized Product Distribution (%). Temperature: 630 Kelvin (365^{o}C).

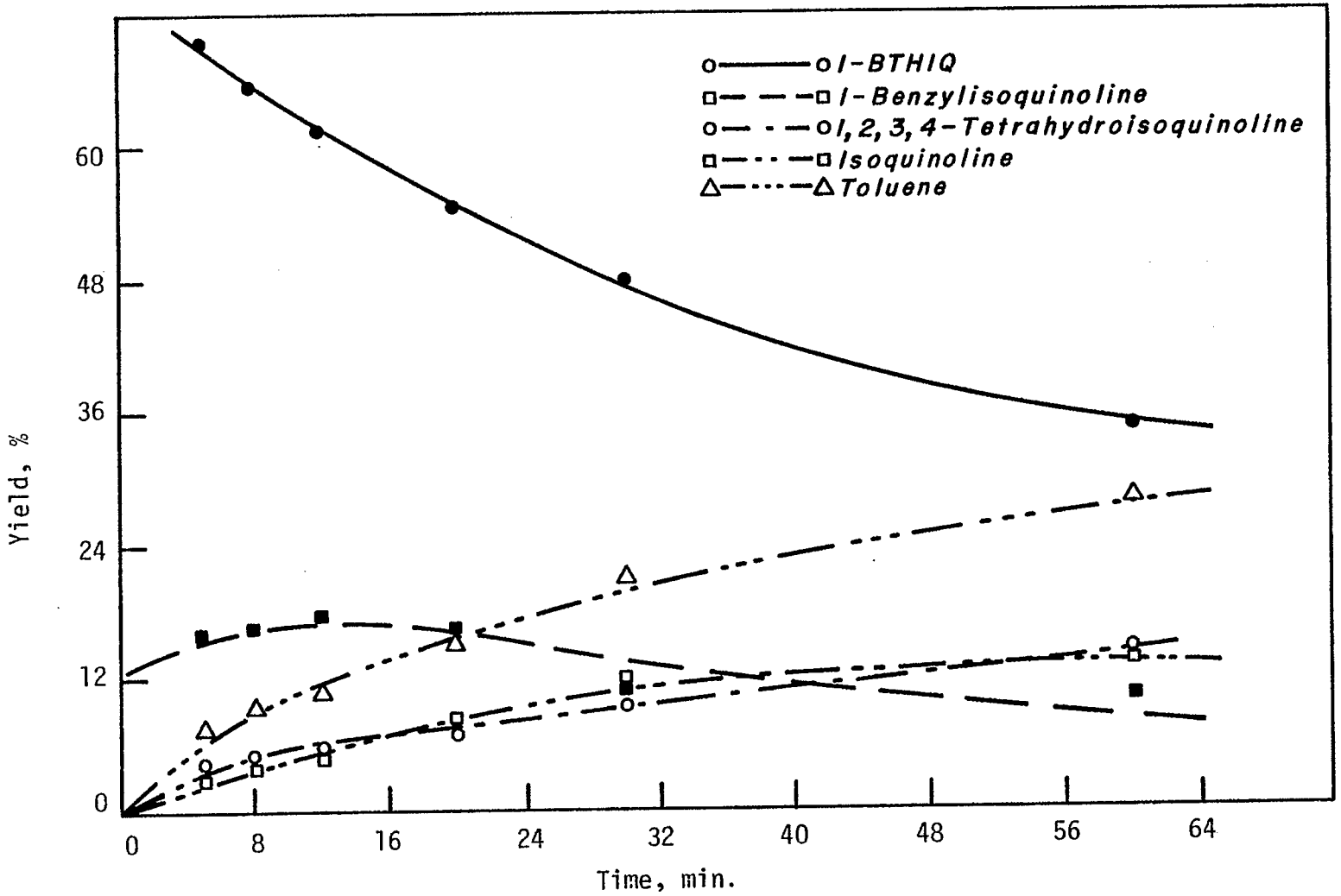

Figure 2. Pyrolysis of 1-Benzyl-1,2,3,4-tetrahydrosioquinoline (1-BTHIQ). Normalized Product Distribution (%, Normalized). Temperature: 588 Kelvin (315^{o}C).

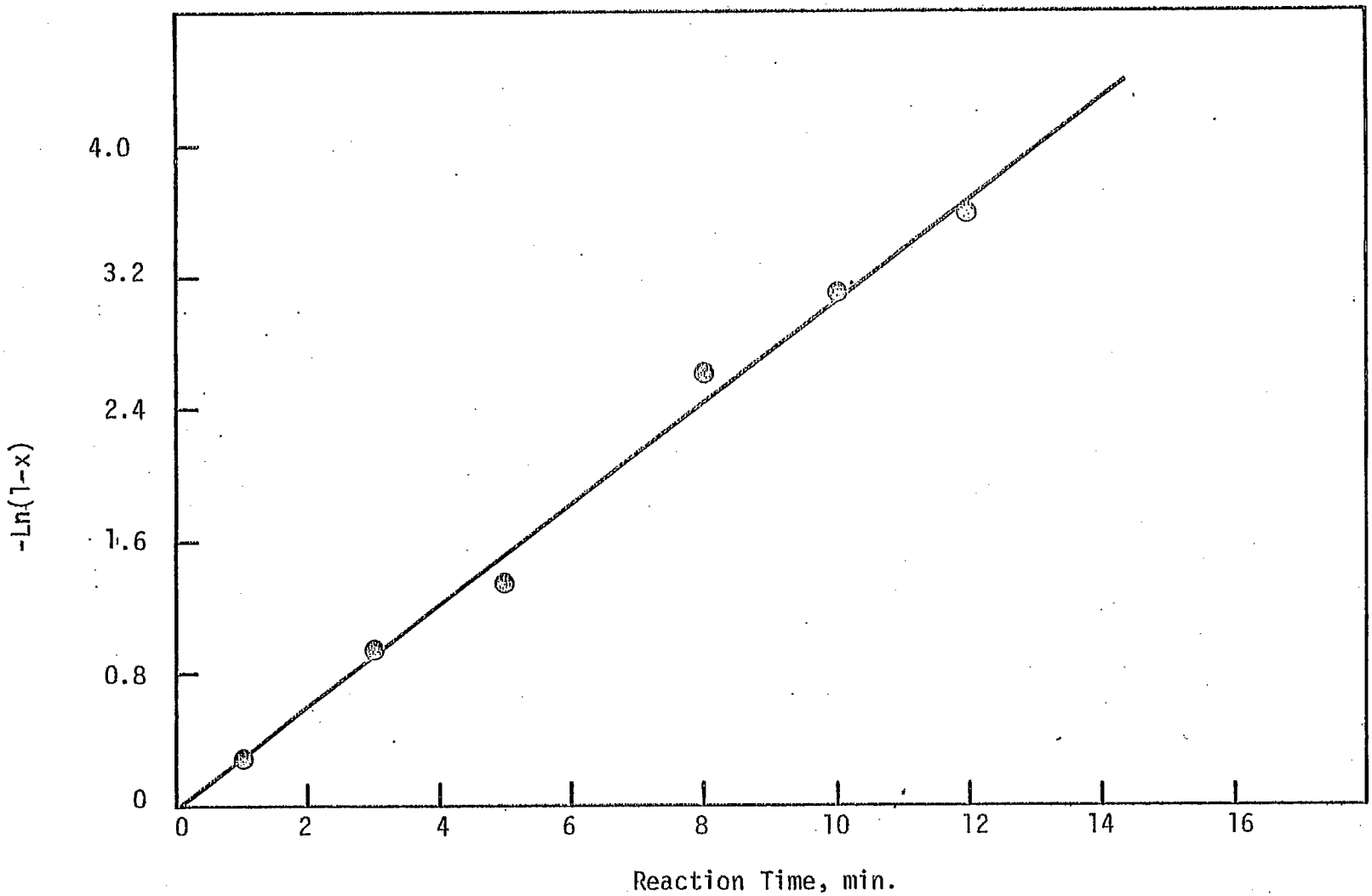

Figure 3. Pyrolysis of 1-Benzyl-1,2,3,4-tetrahydroisoquinoline (1-BTHIQ). First Order Kinetics Plot-Integral Technique. Temperature: 638 Kelvin (365°C).

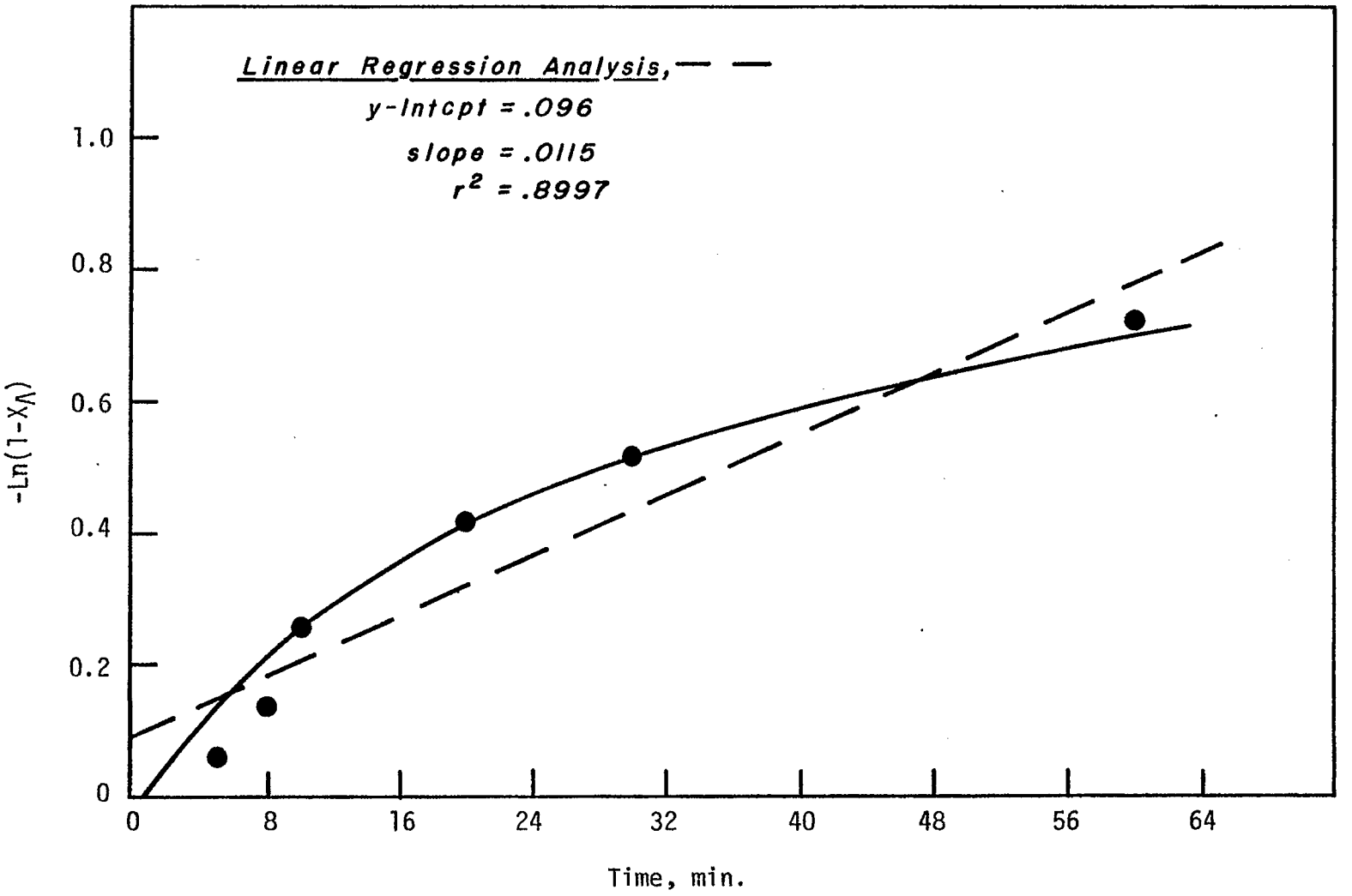

Figure 4. Pyrolysis of 1-Benzyl-1,2,3,4-tetrahydroisoquinoline (1-BTHIQ). First Order Kinetics Plot. Temperature: 588 Kelvin (315°C).

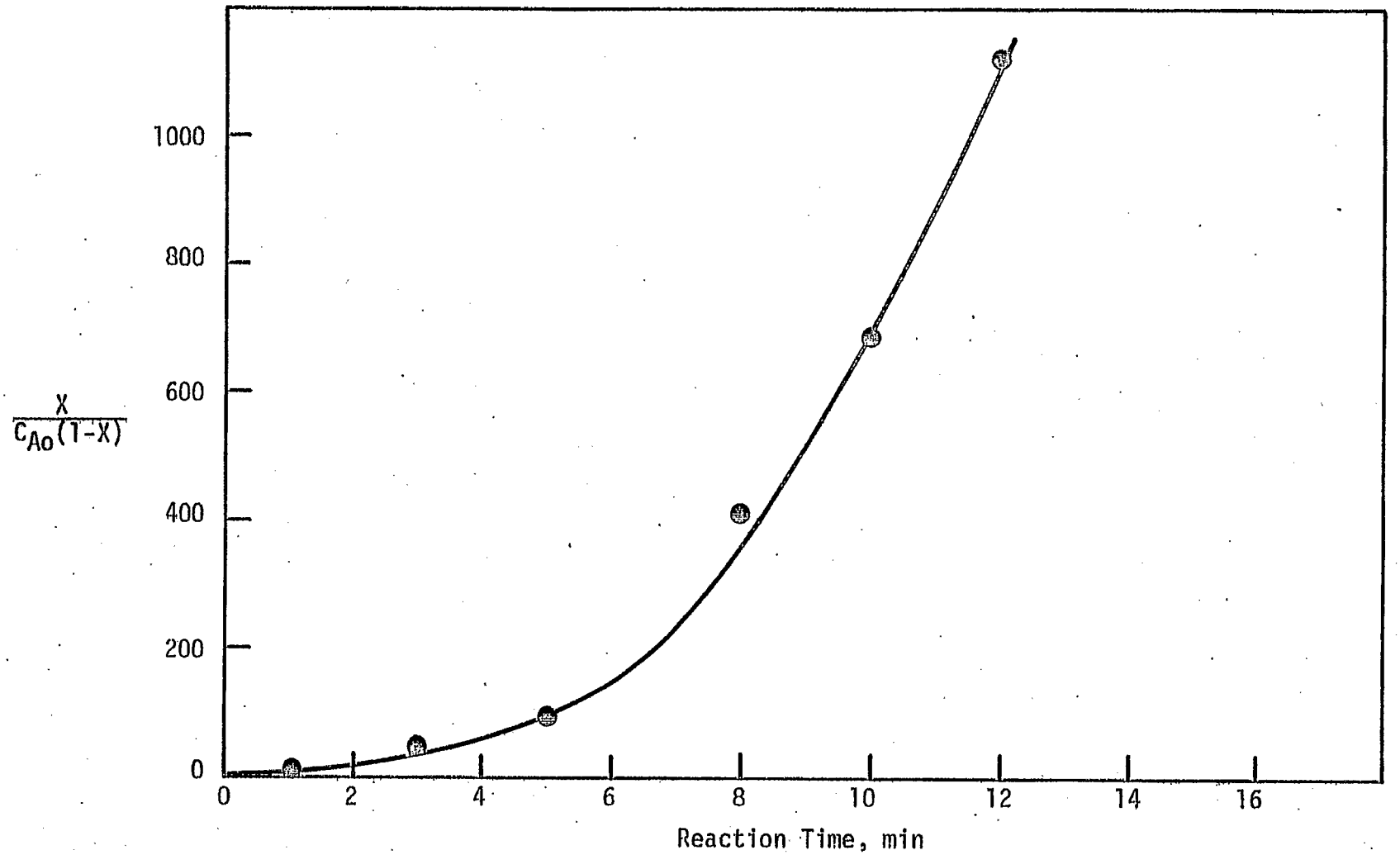

Figure 5. Pyrolysis of 1-Benzyl-1,2,3,4-tetrahydroisoquinoline (1-BTHIQ). Second Order Kinetics Plot-Integral Technique. Temperature: 638 Kelvin (365°C).

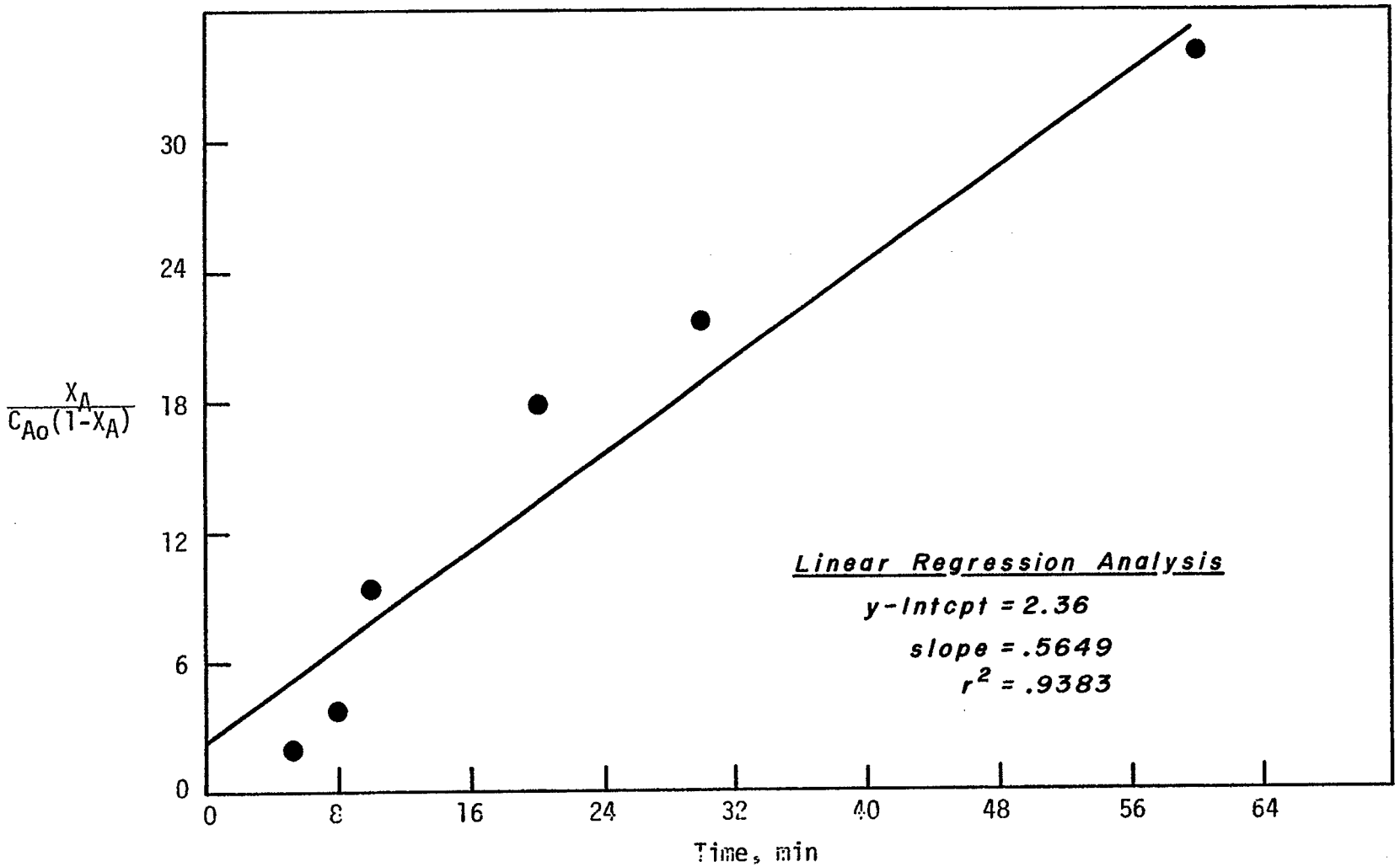

Figure 6. Pyrolysis of 1-Benzyl-1,2,3,4-tetrahydroisoquinoline (1-BTHIQ). Second Order Kinetics Plot. Temperature: 588 Kelvin (315°C).

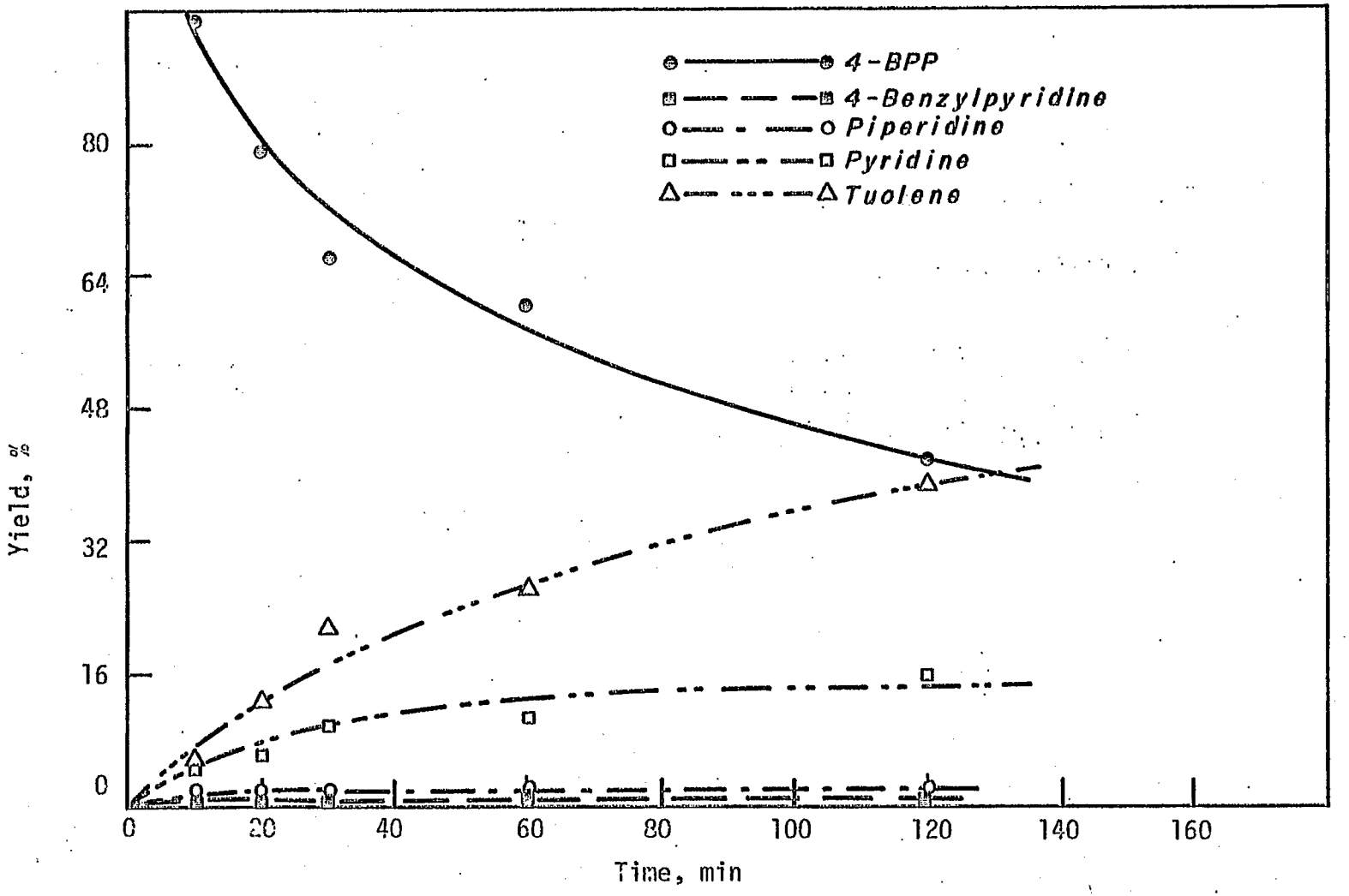

Figure 7. Pyrolysis of 4-Benzylpiperidine (4-BPP).
Normalized Product Distribution (%, Normalized),
Temperature: 673 Kelvin (400°C).

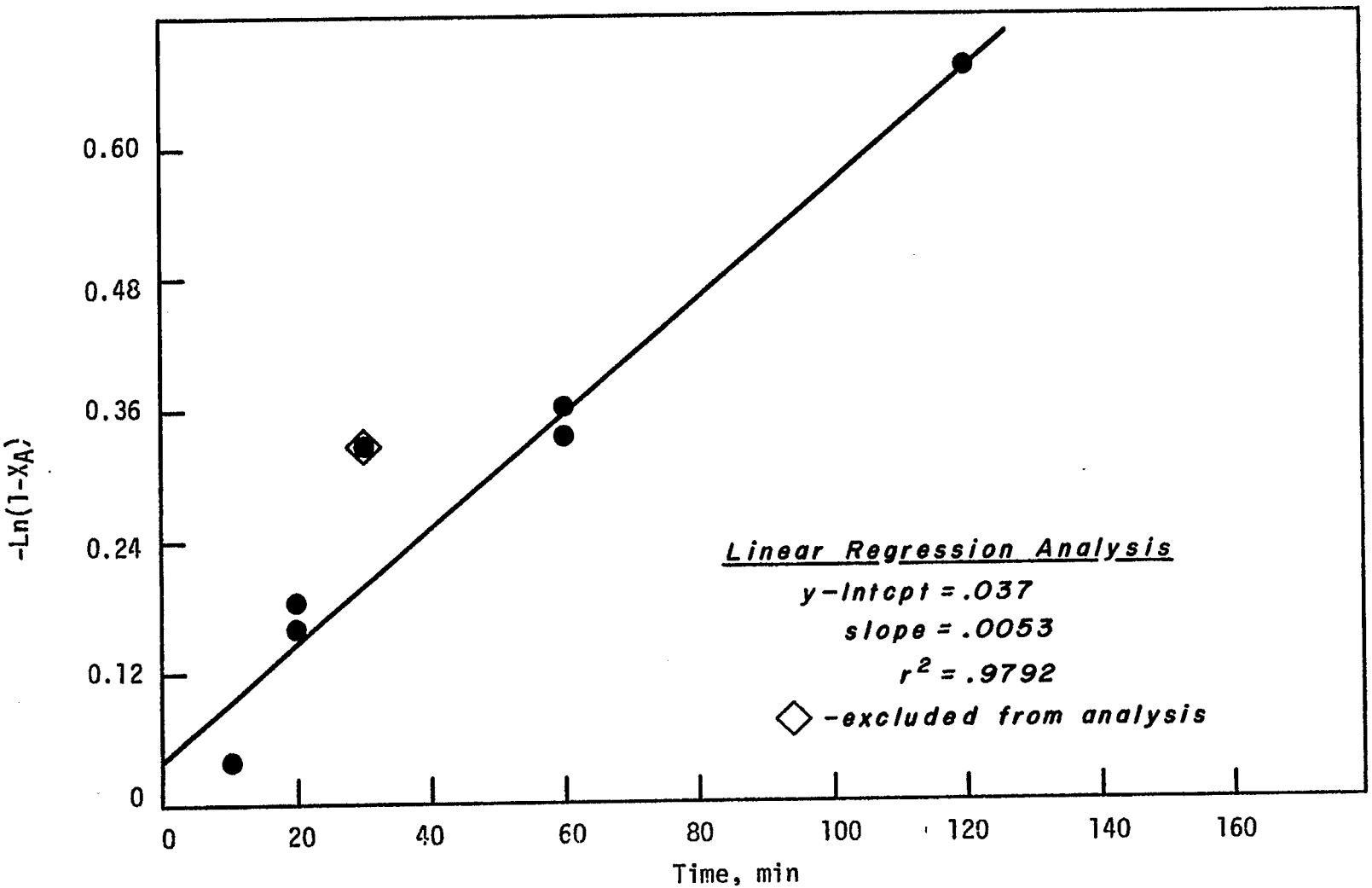

Figure 8. Pyrolysis of 4-Benzylpiperidine (4-BPP). First Order Kinetics Plot. Temperature: 673 Kelvin (400°C).

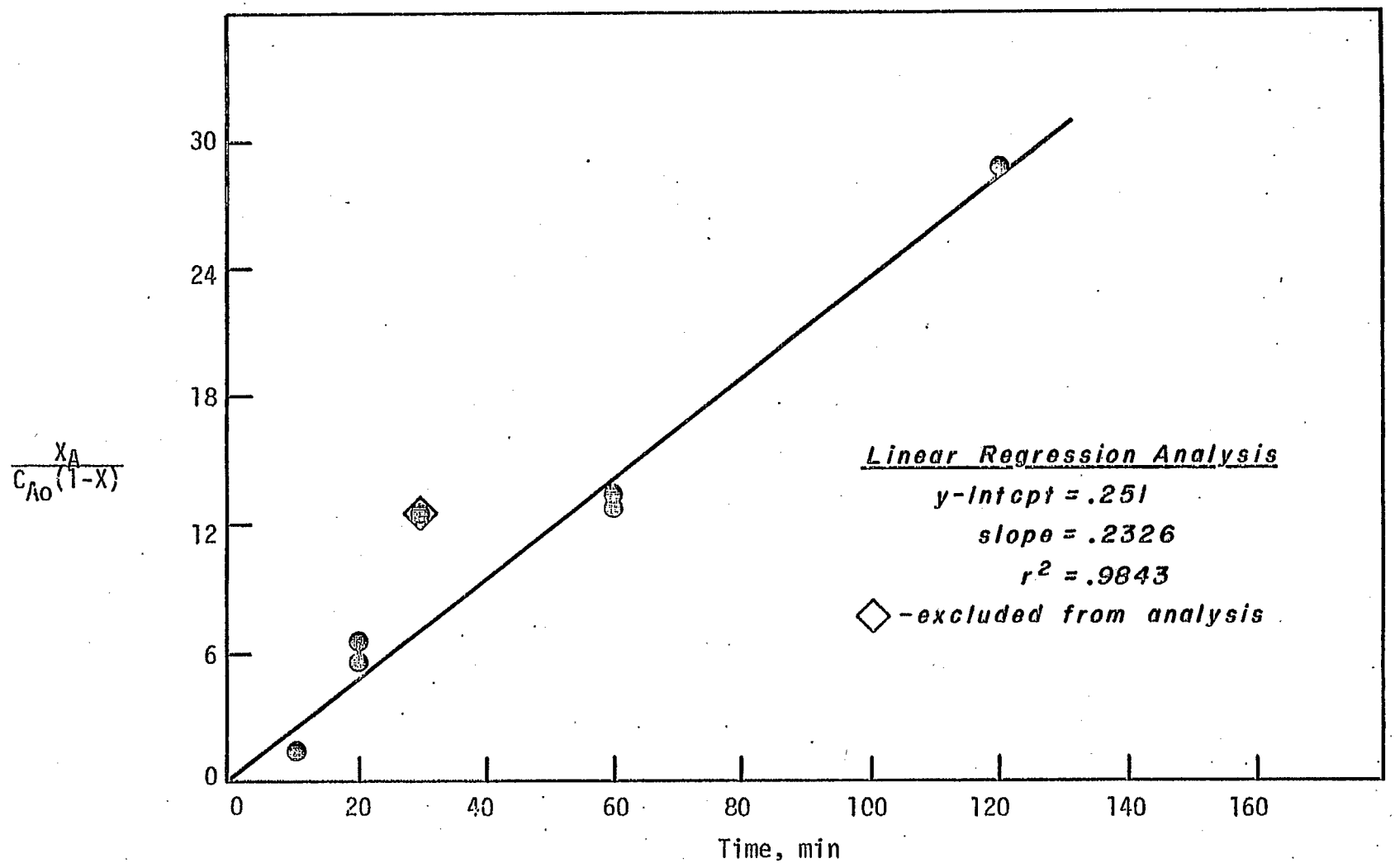

Figure 9. Pyrolysis of 4-Benzylpiperidine (4-BPP). Second Order Kinetics Plot. Temperature: 673 Kelvin (400°C).

Tasks 6, 7, 8 and 9

Tasks 6, 7, 8 and 9 under Dr. J. Shabtai were not submitted on time. These reports will be included in the next Quarterly Progress Report.

Task 10

Systematic Structural Activity Study of Supported Sulfided Catalysts for Coal Liquids Upgrading

Faculty Advisors: F.E. Massoth
J. Shabtai
Post-Doctoral Fellow: N.K. Nag

Graduate Student: K. Baluswamy

Introduction

The objective of this research is to develop an insight into the basic properties of supported sulfide catalysts and to determine how these relate to coal liquids upgrading. The proposed program involves a fundamental study of the relationship between the surface-structural properties of various supported sulfide catalysts and their catalytic activities for various types of reactions. Thus, there are two clearly defined and closely related areas of investigation, viz., (1) catalyst characterization, especially of the sulfided and reaction states and (2) elucidation of the mode of interaction between catalyst surfaces and organic substrates of different types. The study of subject (1) will provide basic data on sulfided catalyst structure and functionality, and would allow the development of catalyst surface models. Subject (2), on the other hand, involves systematic studies of model reactions on sulfide catalysts, and the utilization of data obtained for development of molecular level surface reaction models correlating the geometry (and topography) of catalyst surfaces with the steric conformational structure of adsorbed organic reactants. The overall objective of the project is to provide fundamental data needed for design of specific and more effective catalysts for upgrading of coal liquids.

Atmospheric activity tests using model compounds representative of hydrodesulfurization (thiophene), hydrogenation (hexene) and cracking (isooctene) were employed to assay changes in the catalytic functions of various supported CoMo catalysts. It was found that hydrodesulfurization (HDS) and hydrogenation (HYD) activities were generally unaffected by the type of alumina used or by the cobalt salt used in the preparation; whereas, cracking (CKG) activity varied considerably. Increase in Co or Ni content at a fixed Mo content of 8% resulted in considerably higher promotion of HDS activity than HYD activity. Addition of additives at 1/2% level to the standard $CoMo/Al_2O_3$ catalyst generally increased HDS and CKG for acidic additives and decreased these functions for basic additives, HYD being unaffected. At 5% level, the additives decreased all functions, basic additives decreasing activities more severely. In a series of catalysts employing silica-alumina as the support, the HDS and hydrogenation functions decreased with increasing silica content, while cracking went through a maximum in activity. Catalysts prepared by supporting CoMo on TiO_2, SiO_2-MgO and carbon showed low activities, except for high cracking activity for the two former catalysts.

Oxide precursors of CoMo and Mo catalysts supported on various silica-aluminas evaluated by ESCA showed that support-active component interaction decreased with increase of silica in the support. It was also found that cobalt did not influence the Mo dispersion. On alumina, the Mo phase was found to be dispersed in essentially a monoatomic form.

Several catalyts, which were evaluated in the atmospheric pressure test unit, were subsequently tested at elevated pressure (35 atm) using dibenzothiophene (HDS), naphthalene (HYD) and indole (HDN). The high pressure runs were carried out sequentially in the order indicated to assess the separate catalytic functionalities. Repeat runs of HDS and HYD after HDN gave appreciably lower activities for HDS and HYD which was found to be due to strongly adsorbed residues containing nitrogen. The effect of increasing H_2S was to appreciably decrease HDS, moderately decrease HYD, and moderately increase HDN conversions. The kinetics of the various reactions were successfully modelled with a Langmuir-Hinshelwood rate equation, which included inhibition terms for reactant, products and H_2S.

Stereochemical studies of the hydrogenation of naphthalene and quinoline over several sulfided CoMo, NiMo and NiW catalyts have revealed unusually high trans/cis ratios in the hydrogenated products. Catalyst composition had only a minor effect on these ratios for naphthalene. Methyl substituents on quinoline led to changes in the stereospecific hydrogenation. The active hydrogenation site may consist of a vacancy in the MoS_2 structure into which the molecule adsorbs, the hydrogen atoms being added from opposite sites, in constrast to the flat adsorption on metal sites.

Project Status

Studies to evaluate catalytic functionalities of a 3% Co-8% Mo/Al_2O_3 catalyst with mixed feeds were undertaken in this period. Experiments were carried out in the fixed-bed, flow reactor at 35 atm and 275-375°C. The catalytic functions evaluated were hydrodesulfurization (HDS), hydrogenation (HYD), hydrodeoxygenation (HDO), and hydrodenitrogenation (HDN), using the following model compounds: debenzothiophene (DBT), naphthalene (NAP), dibenzofuran (DBF), and indole (IND), respectively.

Results for binary feeds of the various reactants are presented in Tables 1-3. Conversions of DBF and IND in these tables represent the first bond-breaking step for C-O and C-N, respectively, rather than to hydrocarbon products to better assess the hydrogenolysis sites responsible for these reactions, since the complete removal of the heteroatom in these cases also involves hydrogenation steps. A new charge of catalyst was used for each series. Conversions of duplicate runs gave a relative error of about 5%.

When NAP was added to each of the other reactants (Table 1), their respective conversions were not affected from that of the individual reactants, as judged from previous data. However, the hydrogenation of NAP was decreased in each case in the order: IND > DBT > DBF. The results indicate competitive adsorption effects of the various reactants and/or products for

HDS sites present on the catalyst, and a lack of adsorption of NAP on sites responsible for HDS, HDO and/or HDN. An anomolous temperature inversion in NAP conversion was obtained when DBF was present, viz., lower conversion at 375°C than 350°C. This may be due to retardation of HYD by adsorption of DBF reaction products which are formed at greater amounts at the higher temperature. It is interesting that the HYD of NAP was not affected by additional H_2S (from the excess CS_2) when IND was present, contrary to the decrease in conversion found previously with NAP alone.[1] The higher temperature employed with the mixture may be responsible for the difference.

The results of DBT added to each of the other reactants are given in Table 2. The effect of NAP on the HDS of DBT was negligible, in agreement with the data of Table 1. The effect of DBF and IND cannot be presently evaluated because the HDS of DBT itself has not been run at 350°C and 375°C. Increased H_2S in the feed with IND caused a lowering in HDS, in agreement with earlier results for DBT alone.[1] The effect of DBT on the conversions of the other reactants was more complex, viz., HYD of NAP was decreased, HDO of DBF was increased, and HDN of IND was essentially unchanged. The promotion of HDO converison was unexpected, and is contrary to a recent study using a batch reactor in which DBT was found to slightly lower the HDO of DBF over a $NiMo/Al_2O_3$ catalyst.[2] Increased H_2S enhanced HDN, in line with previous results for IND alone.[1]

Table 3 presents results with a DBF-IND mixture. It is obvious that IND has a very strong inhibiting effect on the HDO of DBF, while the inhibiting effect of DBF on the HDN of IND is considerably less. These results are similar to those reported for a m-cresol-IND mixture.[3] Increased CS_2 in the DBF-IND mixture caused a lowering in HDO and an increase in HDN.

In summary, significant differences in interactions between the reactants in the various binary mixtures were observed. Naphthalene had the least effect and indole the greatest on conversions of the other compounds. This is in line with their relative adsorption strengths. The presence of interactions could indicate that common active sites are used for all the reactions. However, in view of the different responses to H_2S, it is possible that different sites are utilized for the different reactions, even though other (unreactive) compounds could adsorb on these sites. These results indicate that separate model compound reaction studies are insuffient to properly assess the various catalytic functionalities present on different sulfided catalysts.

Future Work

Work on this project has terminated.

References

1. W.H. Wiser et al., DOE Contract No. DE-AC01-79ET14700, Quarterly Progress Report, Salt Lake City, Utah, July-Sept 1982.

2. E. O. Odebunmi and D.F. Ollis, J. Catal. 80, 56 (1983).

3. S. Krishnamurthy and Y.T. Shah, Chem. Eng. Commun. 16, 109 (1982).

Table 1. Conversions for mixtures containing napthalene.

		% HYD Conversion at Liquid Feed of	
Mixture	Temp. °C	7.0 ml/h	10.0 ml/h
NAP	277	77.0	63.0
NAP	350	92.0	91.0
NAP + DBT	277	42.3	25.5
NAP + DBF	375	81.5	80.0
NAP + DBF	350	86.8	83.5
NAP + IND	350	30.0	22.4
NAP + IND + CS_2[a]	350	30.0	22.4
		% Conversion of Second Component at	
Second Component	Temp. °C	7.0 ml/h	10.0 ml/h
DBT	277	70.5	42.5
DBF	375	64.0	45.0
DBF	350	33.5	21.0
IND	350	67.7	56.0
IND + CS_2[a]	350	80.0	70.5

[a]A 3-fold increase in CS_2 added to the feed.

Table 2. Conversions for mixtures containing dibenzothiophene.

Mixture	Temp. °C	% HDS Conversion at Liquid Feed of 7.0 ml/h	10.0 ml/h
DBT	277	66.0	40.3
DBT + NAP	277	62.5	38.5
DBT + DBF	375	94.5	92.5
DBT + IND	350	86.0	77.5
DBT + IND + CS_2[a]	350	74.5	62.2
Second Component	**Temp. °C**	**% Conversion of Second Component at 7.0 ml/h**	**10.0 ml/h**
NAP	277	37.0	25.5
DBF	375	79.0	67.2
IND	350	70.0	57.8
IND + CS_2[a]	350	79.5	71.5

[a]A 3-fold increase in CS_2 added to the feed.

Table 3. Conversions for mixture of dibenzofuran and indole.

Mixture	Temp. °C	% HDO Conversion at Liquid Flow of 7.0 ml/h	10.0 ml/h
DBF	375	67.0	49.5
DBF + IND	375	3.5	2.0
DBF + IND	350	1.5	1.5
DBF + IND + CS_2[a]	350	<1.5	<1.5
Second Component	**Temp. °C**	**% Conversions of Second Component at 7.0 ml/h**	**10.0 ml/h**
IND	375	83.0	76.0
IND	350	53.0	44.0
IND + CS_2[a]	350	69.0	61.5

[a]A 3-fold increase in CS_2 added to the feed.

Task 13

Catalyst Research and Development

Synthesis of Light Hydrocarbons from CO and H_2

Faculty Advisor: F.V. Hanson
Graduate Student: Y.S. Tsai

Introduction

The production of low molecular weight olefins (C_2-C_4) from the hydrogenation of carbon monoxide has been investigated over unsupported iron-manganese catalysts. The results from the preliminary tests which were performed in a bench-scale fixed-bed reactor system showed that the unsupported iron-manganese catalysts were very selective in the production of C_2-C_4 olefins. Data from the screening tests of the sixteen iron-manganese catalysts indicated that a catalyst composed of 2 parts of manganese per 100 parts of iron was the most selective. The effects of the process variables were also studied. The results essentially agreed with those reported in the literature.

The influence of the total pressure on the catalyst activity and selectivity has been investigated. However, the effect of the reactant partial pressure is still unclear. In this study there are only two reactants in the synthesis gas, hydrogen and carbon monoxide. The partial pressure of the hydrogen was maintained at a constant value while the partial pressure of the carbon monoxide varied. When the partial pressure of the carbon monoxide was maintained, the partial pressure of the hydrogen varied. The preliminary data indicated that the catalyst activity increased as the hydrogen partial pressure increased. However, an increase in the carbon monoxide partial pressure resulted in a lower catalyst activity.

The selectivities for C_2-C_4, C_5^+ and ROH were generally constant in spite of the partial pressure change, but the O/P ratio of the C_2-C_4 hydrocarbons was higher with the lower H_2 pressure and the higher CO pressure.

Project Status

A constant temperature of 225°C and a fixed space velocity of 1.33 $cm^{-3}g^{-1}sec^{-1}$ were used for all experiments. The total pressure of the synthesis gas and the H_2/CO ratio were adjusted simultaneously to obtain a constant H_2 (or CO) partial pressure with varying CO (or H_2) partial pressures. A FT-5 Fe-Mn coprecipitated catalyst with an atomic ratio of 11.8 Mn/100 Fe was used. The catalyst was reduced with H_2 at 400°C for 8 hours and activated with a synthesis gas of $2H_2/CO$ for 12 hours to achieve a stable production level.

Table 1 shows the effect of the hydrogen partial pressure on the catalyst activity and selectivity. The CO conversion increased from 2.0% to 9.3% as the hydrogen partial pressure increased from 106.3 psia to 318.9 psia with a constant CO partial pressure of 106.3 psia. An increase in H_2 partial pressure also accompanied a decrease in CO_2 production and an increase in the selectivity for CH_4. The selectivities for C_2-C_4, C_5^+ and ROH were generally constant at 46.0%, 15.0% and 3.0%, respectively, in spite of the partial pressure change. However, the O/P ratio of the C_2-C_4 hydrocarbons declined with an increase in the H_2 partial pressure.

The effect of the CO partial pressure on the catalyst activity and selectivity is shown in Table 2. The CO conversion decreased from 13.1% to 3.2% as the CO partial pressure increased from 85.4 psia to 256.3 psia. The selectivities for C_2-C_4 and ROH were generally constant at 46.5% and 3.0%, respectively, but the O/P ratio of the C_2-C_4 hydrocarbons increased as the CO partial pressure increased. The increase of CO_2 and C_5^+ production and the decrease in CH_4 selectivity were due to the increase in the CO partial pressure. It is consistent in both experiments to say that the increase in the CO conversion and the CH_4 production as well as the decrease in the CO_2 production and the O/P ratio of the C_2-C_4 hydrocarbons were influenced by the increase in the H_2/CO ratio of the synthesis gas. These results agreed with those in the previous investigation.

Future Work

A catalyst characterization study will be initiated. A literature survey on CO hydrogenation as well as heat and mass transfer for the fixed-bed reactor will be continued.

Table 1. Effect of hydrogen partial pressure on the product yield and selectivity; 225°C, 1.33 $cm^{-3}g^{-1}sec^{-1}$ space velocity, FT-5 Fe-Mn catalyst (11.8 Mn/100 Fe atomic ratio).

Total Pressure (psia)	212.6	318.9	425.2
CO Partial Pressure (psia)	106.3	106.3	106.3
H_2 Partial Pressure (psia)	106.3	212.6	318.9
H_2/CO Ratio	1	2	3
CO Conversion (%)	2.0	4.0	9.3
Selectivity (%) CO_2	18.3	13.4	10.6
Selectivity (%) C_1	18.4	22.0	23.2
Selectivity (%) C_2-C_4	44.2	46.8	47.9
Selectivity (%) C_5^+	15.8	15.0	15.5
Selectivity (%) ROH	3.3	2.8	2.8
O/P in C_2-C_4	5.91	5.82	4.76

Table 2. Effect of carbon monoxide pressure on the product yield and selectivity; 225°C, 1.33 $cm^3g^{-1}sec^{-1}$ space velocity, FT-5 Fe-Mn catalyst (11.8 Mn/100 Fe atomic ratio).

Total Pressure (psia)	341.7	384.5	512.6
H_2 Partial Pressure (psia)	256.3	256.3	256.3
CO Partial Pressure (psia)	85.4	128.2	256.3
H_2/CO Ratio	3	2	1
CO Conversion (%)	13.1	4.5	3.2
Selectivity (%) CO_2	9.9	13.4	17.4
Selectivity (%) C_1	28.1	19.8	14.2
Selectivity (%) C_2-C_4	45.9	48.1	47.3
Selectivity (%) C_5^+	13.4	15.4	18.1
Selectivity (%) ROH	2.7	3.3	3.0
O/P in C_2-C_4	3.50	4.28	5.47

Task 13

Catalyst Research and Development

Hydrogenation of Carbon Monoxide over Raney Fe-Mn Catalyst

Faculty Advisor: F.V. Hanson
Graduate Student: K.R. Chen

Introduction

The objectives of this project are to determine the kinetics of the caustic leaching of alumina from iron-aluminum alloys and to determine the optimum process operating conditions for the production of low molecular weight of the olefins from hydrogen and carbon monoxide over Raney iron-manganese catalysts.

A single phase Al-Fe (53/47 wt %) alloy was prepared for the leaching kinetics study. The leaching conditions were: leaching temperature, 303 - 353 K; alloy granule particle size, 30 - 325 mesh, 5% NaOH and alloy sample size, 5 g. The volumetric flow rate of the hydrogen evolved was determined with a wet test meter.

A Raney iron-manganese catalyst, prepared from an Al-Fe-Mn (59/38/3, 363 leaching) alloy, was used to evaluate the activity and selectivity of the catalyst. Catalyst loading and stability tests were conducted prior to the process variable study.

Project Status

The M.S. Thesis of Mr. K.R. Chen is being completed and a copy will be submitted when finished.

Future Work

The Raney iron-manganese catalyst in the slurry bed reactor system will be used to optimize the C_2-C_4 olefinic products.

V. Conclusion

Detailed conclusions are included in the reports for each task. Task 4 is no longer funded and has been discontinued. No reports were submitted for Tasks 6, 7, 8, and 9. Tasks 11, 12 and 14 are inactive. No work was done under Task 15.